UNIVERSITY OF CALIFORNIA
RIVERSIDE

Spatiotemporal Neuroprotection and Early Regeneration after Ischemic Stroke with Neuregulin-1 Treatment

A Dissertation submitted in partial satisfaction
of the requirements for the degree of

Doctor of Philosophy

in

Biomedical Sciences

by

Jessica M. Noll

September 2021

Dissertation Committee:
Dr. Byron D. Ford, Chairperson
Dr. Monica Carson
Dr. Iryna Ethell

The Dissertation of Jessica M. Noll is approved:

_____

_____

_____

Committee Chairperson

University of California, Riverside

Acknowledgements

The text of this dissertation, in part, is a reprint of the material as it appears in the Journal of Molecular Neuroscience 2019. The coauthor Byron Ford listed in that publication directed and supervised the research which forms the basis for this dissertation. The coauthors, Yonggang Li and Timothy J. Distel listed in that publication contributed to acquisition of data for that publication. The coauthor, Gregory D. Ford listed in that publication contributed to the conception and design of the work within that publication.

Gratitude for financial support for my education includes the Biomedical Sciences Division, the University of California, Riverside Graduate Division, the National Institute of Health Neurological Disorders and Stroke Division, the National Science Foundation, and the W.M. Keck Foundation.

To my advisor, Dr. Byron D. Ford, for his invaluable support, endless patience, and amazing mentorship. Thank you for teaching me how to continue to ask questions, how to adapt to unexpected results, and how to overcome barriers in research and in life. I have become a stronger, more resilient person because of you, and I will always admire you as a mentor and as a person for that, thank you.

To my committee members, Dr. Monica Carson and Dr. Iryna Ethell, for always believing in and supporting me throughout my research career. Thank you for your years of tough mentorship and building my ability to become an independent, confident researcher. I could not be the researcher I am today without your expertise, critique, and invaluable advice, thank you.

ABSTRACT OF THE DISSERTATION

Spatiotemporal Neuroprotection and Early Regeneration after Ischemic Stroke with Neuregulin-1 Treatment

Jessica M. Noll

Doctor of Philosophy, Graduate Program in Biomedical Sciences
University of California, Riverside, September 2021
Dr. Byron Ford, Chairperson

Stroke is ranked as the fifth leading cause of death and the leading cause of adult disability. Unfortunately, Tissue Plasminogen Activator is the only FDA approved stroke treatment but does not address acute injury or cerebral recovery. Neuregulin-1 (NRG-1) has demonstrated promise as an acute neuroprotective, anti-inflammatory, and neuroregenerative agent in animal stroke models. In this dissertation, we examined the spatial cellular and inflammatory mechanisms occurring early after ischemic stroke and with NRG-1 treatment. Exogenous NRG-1 treatment administered to C57bl/6 male and female mice via intra-arterial or intravenous routes significantly reduced cerebral cortical infarct volume, inhibited neuronal injury, and reduced apoptosis at 24-hours after MCAO. Neuroprotection by endogenous NRG-1 was also seen as male and female heterozygous NRG-1 (NRG-1 +/-) knockout mice demonstrated a sixfold increase in cortical infarct size compared to wild-type mice. Immunohistochemistry and Nanostring Digital Spatial Profiling (DSP) were then utilized to characterize the spatial mechanisms occurring early after ischemia and determine if NRG-1 plays a therapeutic role in a similar spatial manner. Male C57bl/6 mice were given a photothrombotic MCAO and sacrificed at three-days post-ischemia. We demonstrated that the ipsilateral hemisphere initiates distinct spatial regulatory proteomic profiles that can be identified

consistently with the immunohistochemical markers, FJB, GFAP, and Iba-1. DSP defined the core border profile as inducing neuronal death, apoptosis, immunoreactivity, and early degenerative proteins. The peri-infarct induced astrocytic immunoreactivity, autophagy, and neurodegenerative proteins, while the peri-infarct normal tissue demonstrated minimal changes. These profiles were then analyzed after daily NRG-1 treatment beginning at 24-hours after ischemic onset. We found no difference in FJB, Iba-1, or GFAP expression between treatment groups. However, delayed daily NRG-1 treatment induced proteomic changes indicating restoration of autophagy and mitophagy within neurons and myeloid cells within the ischemic core border and peri-infarct regions as early as three days post-ischemia, suggesting neuronal resistance to apoptosis and priming for an anti-inflammatory and neuroregenerative niche. Therefore, we identify NRG-1 as a potent ischemic therapeutic capable of inducing immediate and late neuroprotection, early neuroregeneration, and extending the therapeutic treatment window.

Table of Contents

	Page
Title	**i**
Copyright	**ii**
Signature Approval	**iii**
Acknowledgments	**iv**
Abstract	**v**
Table of Contents	**vii**
List of Abbreviations	**ix**
List of Figures	**xi**
List of Tables	**xiv**
Chapter 1: Introduction and Literature Review	
1.1 Background	1
1.2 Ischemic Injury and Implication for Neuroprotection	2
1.3 Neuregulin-1 as a Neuroprotectant Target	2
1.4 Neuregulin-1 as an Anti-inflammatory Agent	4
1.5 Spatiotemporal Regulation and Repair	4
1.6 Neuregulin-1 and Clinical Progress	5

Chapter 2: Neuroprotection by Exogenous and Endogenous Neuregulin-1 in Mouse Models of Focal Ischemic Stroke

2.1 Introduction 6

2.2 Materials and Methods 7

2.3 Results 11

2.4 Discussion 18

Chapter 3: Spatial Analysis of Neural Cell Proteomic Profiles following Ischemic Stroke in Mice using High-Plex Digital Spatial Profiling

3.1 Introduction 20

3.2 Materials and Methods 21

3.3 Results 27

3.4 Discussion 38

Chapter 4: Delayed Neuregulin-1 Treatment Induces a Late Neuroprotective and Early Regenerative Proteomic Profile

4.1 Introduction 42

4.2 Materials and Methods 43

4.3 Results 48

4.4 Discussion 59

Chapter 5: Conclusion and Overall Discussion 63

Bibliography and References 66

List of Abbreviations

BBB	Blood-brain barrier
BSA	Bovine serum albumin
CBF	Cerebral blood flow
DPI	Days post-ischemia
DSP	Digital spatial profiling
ECA	External carotid artery
FDA	Food and drug administration
FFPE	Formalin-fixed paraffin embedded
FJB	Fluoro-jade B
i.a.	Intra-arterial
i.p.	Intraperitoneal
i.v.	Intravenous
IACUC	Institutional animal care and use committee
ICA	Internal carotid artery
KMnO4	Potassium permanganate
LDF	Laser doppler flowmetry
MCAO	Middle cerebral artery occlusion

NRG-1	Neuregulin-1
PBS	Phosphate-buffered saline
PFA	Paraformaldehyde
PiNT	Peri-infarct normal tissue
pMCAO	Permanent middle cerebral artery occlusion
PtMCAO	Photothrombotic middle cerebral artery occlusion
ROI	Region(s) of interest
SCI	Spinal cord injury
STAIR	Stroke treatment academic industry roundtable
tMCAO	Transient middle cerebral artery occlusion
tPA	Tissue plasminogen activator
TTC	Triphenyl tetrazolium chloride
TUNEL	Terminal deoxynucleotidyl transferase dUTP nick end labeling
WT	Wild-type

List of Figures

Page

Chapter 2: Neuroprotection by Exogenous and Endogenous Neuregulin-1 in Mouse Models of Focal Ischemic Stroke

Figure 2.1 Neuroprotection with intra-arterial NRG-1 treatment shown by TTC 12

Figure 2.2 NRG-1 does not affect regional CBF after MCAO 13

Figure 2.3 NRG-1 does not affect animal body temperature or weight after MCAO 13

Figure 2.4 NRG-1 reduced FJB staining in the brain following MCAO/reperfusion 14

Figure 2.5 NRG-1 blocks ischemia induced apoptosis 15

Figure 2.6 NRG-1 protects neurons from ischemic damage following MCAO/reperfusion 15

Figure 2.7 NRG-1 reduced infarct volume via intravenous administration in male and female mice 16

Figure 2.8 Endogenous NRG-1 protects neurons following MCAO/reperfusion 17

Chapter 3: Spatial Analysis of Neural Cell Proteomic Profiles following Ischemic Stroke in Mice using High-Plex Digital Spatial Profiling

Figure 3.1 Representative Stereotaxic Locations and Regions of Interest at 3-days Post-Ischemia 25

Figure 3.2 Neuronal Damage 3-Days post-Ischemia 28

Figure 3.3 GFAP Expression Increases in Core Border 3 Days Post-Ischemia 30

Figure 3.4 Iba-1 Expression Demonstrates Microglia Reactivity 3 Days Post-Ischemia 31

Figure 3.5 Histological Markers Define Core Border at 3 Days Post-Ischemia 33

Figure 3.6. Representative Immunohistochemical Figures for DSP Analysis and ROI Selection 34

Figure 3.7 Ischemia Presents Region Specific Proteomic Profiles 35

Figure 3.8 Hierarchical Cluster Heat Map of ROIs 36

Chapter 4: Delayed Neuregulin-1 Treatment Induces a Late Neuroprotective and Early Regenerative Proteomic Profile

Figure 3.1 Representative Stereotaxic Locations and Regions of Interest at 3-days Post-Ischemia 25

Figure 4.1 FJB Demonstrates No Difference with NRG-1 Treatment at 3 Days Post-Ischemia 49

Figure 4.2 GFAP Demonstrates No Difference with NRG-1 Treatment at 3 Days Post-Ischemia 51

Figure 4.3 Iba-1 Demonstrates No Difference with NRG-1 Treatment at 3 Days Post-Ischemia 52

Figure 4.4 Representative Immunohistochemical Figures for DSP Analysis and ROI Selection 53

List of Tables

Chapter 3: Spatial Analysis of Neural Cell Proteomic Profiles following Ischemic Stroke in Mice using High-Plex Digital Spatial Profiling

Table 3.1	Tissue-Tek Processing Protocol	26
Table 3.2	Regulatory Proteomic ROI Profiles	38

Chapter 4: Delayed Neuregulin-1 Treatment Induces a Late Neuroprotective and Early Regenerative Proteomic Profile

Table 3.1	Tissue-Tek Processing Protocol	47
Table 4.2	Delayed NRG-1 Treatment Induces a Late Neuroprotective and Early Regenerative Profile 3-Days After Ischemic Stroke	59

Chapter 1: Introduction and Literature Review

1.1 Background Stroke remains one of the most devasting diseases in modern healthcare. Previously ranked as the third leading cause of death, stroke has since decreased to fifth but remains the leading cause of adult disability (Lloyd-Jones 2010; Benjamin 2017). There are two major classifications of stroke: ischemic, which is the occlusion or blockage of an artery within the brain, and hemorrhagic, which is a rupture of an artery within the brain and leads to subsequent bleeding into the surrounding tissue. Approximately 795,000 strokes occur in the United States (U.S.) alone every year with 80% of strokes classifying as ischemic (Benjamin 2017).

There is currently only one FDA-approved treatment for stroke, tissue plasminogen activator (tPA), a thrombolytic used for ischemic stroke (Lapchak 2013). Unfortunately, t-PA has a limited time window for therapeutic use, and only 3–5% of stroke patients arriving at the hospital will qualify for treatment (Fisher 2009). Importantly, as stroke progression is recognized to be a complex integration of glia, neurons, and the surrounding extracellular matrix, treatments must target the detrimental effects created by these interactions (Jeong 2013; Detante 2014; Jayaraj 2019). tPA treatment does not play a neuroprotective or anti-inflammatory role, and is not ideal for prevention of secondary, long-term neurodegenerative damage. Several potential neuroprotective agents, including glutamate antagonists, anti-inflammatory compounds, free radical scavenging agents and hematopoietic growth factors were shown to be effective in preclinical animal models of ischemia, but failed to demonstrate efficacy in clinical trials with human patients following stroke. (O'Collins 2006). Therefore, there is a strong need to understand the cellular and inflammatory mechanisms occurring early after ischemic stroke in a spatial manner in order to develop future ischemic stroke treatments.

1.2 Ischemic Injury and Implication for Neuroprotection Brain ischemia is characterized by early onset neuronal death beginning within minutes following stroke. This initial area of brain injury (the infarct core) is characterized by low cerebral blood flow, energy failure, excitotoxicity, and edema [for reviews, (Dirnagl 1999; Barone 1999)]. The resulting ischemic brain injury is also accompanied by increased synthesis of inflammatory molecules and oxidative stress in neurons, glia, and in the cerebral vasculature, which endangers brain cells in a larger, surrounding area of brain tissue for which the blood supply is compromised but not completely interrupted (del zoppo 2000; Iadecola 2001, 2011; Stoll 1998). This population of surviving, yet vulnerable cells makes up the ischemic penumbra, which surrounds the necrotic core of the infarct (Dirnagl 1999; Touzani 2001). The expansion of the infarct core is a time-dependent situation where damage to the adjacent viable tissue continues to progress into the penumbra. In the penumbra, neurons can survive for several hours following stroke onset, indicating an ideal treatment paradigm for early neuroprotectants. After ischemic damage is complete, the remaining, bordering region of reversibly damaged cells in an area of decreased neuronal density is the peri-infarct tissue (Lipton 1999). The peri-infarct tissue later becomes an important target for neurorepair as a neurogenesis niche, with a growth permissive environment allowing for induction of axonal sprouting, new neuronal connections, and survival and maturation of new neurons (Carmichael 2006). Together, this suggests that the therapeutic window for neuroprotection and repair following stroke can be quite prolonged and potentially a dual-role for early neuroprotectants within the penumbra and later neurorepair targeting peri-infarct mechanisms.

1.3 Neuregulin-1 as a Neuroprotectant Target NRG-1, also known as acetylcholine receptor-inducing activity (ARIA), glial growth factor (GGF), heuregulin and neu differentiation factor (NDF), plays roles throughout the peripheral and central nervous system (Meyer 1997). NRG-1 acts through homo- or heterodimerization of erbB (1-4) receptor tyrosine kinase receptors (Meyer

1997). During development, NRG-1 is required for generation of neurons in cranial ganglia and is necessary for Schwann cell migration, differentiation, and myelination (Meyer 1997). In adulthood, NRG-1 is not necessary for axonal or myelin maintenance but is endogenously released upon nerve injury by neurons and astrocytes for acute protection and regeneration (Fricker 2011a; Parker 2002; Tokita 2001; Eilam 1998). NRG-1 also acts upon oligodendrocytes, Schwann cells, astrocytes, and glia expressing erbB receptors to initiate neuroprotection and regeneration (Fricker 2011a, b; Tokita 2001; Xu 2005, 2006, 2012). Therefore, these studies suggest that NRG-1 plays a potential multiple mechanistic role by acting on many glial types including neurons, oligodendrocytes, and astrocytes that could be crucial for preclinical and clinical success.

ErbB4 is upregulated in injured neurons and has been suggested to increase the capacity to respond to available NRG-1 (Xu 2005; Clement 2007). Exogenous NRG-1 treatment has exhibited acute neuroprotection in stroke models as well as in spinal cord injury (SCI), experimental cerebral malaria, and nerve agent intoxication (Alizadeh 2017; Li 2007, 2012, 2015; Noll 2019). Work from our laboratory and others demonstrated that NRG-1 reduced ischemia-induced neuronal death and inflammation in rodent focal stroke models by ~90% with a therapeutic window of >12 hours (Shyu 2004; Xu 2004, 2006; Li 2007, 2008 2009; Guo 2006; Guan 2015; Noll 2019). In addition, NRG-1 prevented neuronal injury and improved blood-brain barrier (BBB) integrity in animal models of brain hemorrhage (Qian 2018; Yan 2017; Navarro 2019; Lok 2012).

NRG-1 is endogenously released by neurons to induce migration along radial glia during development and provide subsequent trophic support within the peripheral and central nervous system (Buonanno 2001; Barres 1999). This suggests a potential role in stimulating neuronal plasticity and trophic support after brain injury. NRG-1 administration resulted in a significant improvement of neurological function when administered 3 days following ischemia, suggesting a role in neuronal regeneration and repair (Iaci 2016). The study demonstrated that daily intravenous

treatment with a NRG-1 isoform (Glial growth factor 2/neuregulin 1β3) at 1.0mg/kg for ten days increased neural plasticity markers GAP-43 and synaptophysin in the ipsilateral and contralateral somatosensory and motor cortices. Additionally, in a rat SCI model, NRG-1 administered intrathecally continuously for 1-2 weeks enhanced axonal preservation, increased new oligodendrocytes, and attenuated astrogliosis and tissue degeneration (Gauthier 2013). These studies suggest that delayed NRG-1 treatment plays a significant role in neuroregeneration that remains to be elucidated.

1.4 Neuregulin-1 as an Anti-inflammatory Agent We have shown anti-inflammatory effects of NRG-1 in multiple *in vivo* acute brain injury models. NRG-1 prevented macrophage/microglial activation, reactive astrogliosis, apoptosis, and cytokine expression following ischemic stroke (Xu 2004, 2005, 2006; Li 2007). In a rat transient MCAO model, NRG-1 treatment reduced inflammatory and stress genes by 50% or more specifically including IL-1β, cyclooxygenase-2 (COX2), CD36, heat shock protein 70 (HSP-70), and monocyte chemoattractant protein-1 (MCP-1) (Simmons 2016; Xu 2005). In an SCI rat model, NRG-1 decreased neuronal damage and pro-inflammatory markers TNFα, IL-1β, matrix metallopeptidase 2 (MMP2), matrix metallopeptidase 9 (MMP9), nitric oxide (NO), and chondroitin sulfate proteoglycans (CSPGs) while increasing anti-inflammatory markers IL-10 and arginase-1 (Arg-1) (Alizadeh 2017). This suggests that NRG-1 plays an important dual role as a neuroprotectant and an anti-inflammatory agent acutely after ischemic stroke.

1.5 Spatiotemporal Regulation and Repair During stroke recovery, the peri-infarct region is recognized for increased cellular recovery processes and the induction of regenerative factors. The peri-infarct exhibits a complex, dynamic interaction between immune and neuronal cells in both rodents and humans that critically determine repair processes after ischemia (Price 2006; Cramer 2006a). Neuroinflammation after ischemia involves activation of microglia, astrocytes, and

infiltration of peripheral leukocytes (Hallenbeck 1996; Pekny 2005; Kawabori 2015; Kim 2016). Resident microglia demonstrate reactivity with a change in morphology and infiltration into the core (Nowicka 2008; Kawabori 2015; Sanchez-Bezanilla 2021). Astrocytes proliferate and increase expression of inflammatory factors such as glial fibrillary acidic protein (GFAP) which lead to astroglia scar formation along the infarct border (Pekny 2005; Nowicka 2008; Sanchez-Bezanilla 2021). Progressive invasion and inflammatory processes lead to cavitation within the core lesion region (Fitch 1999). Axonal sprouting, neurite outgrowth, and neuroplasticity increase within the periinfarct tissue and gradually spread into the core region (Buga 2014; Brown 2008; Hinman 2013; Carmichael 2006). Neuroinflammatory interactions over a prolonged period can create a complex deteriorating vs neuroprotective/neuroregenerative dynamic roles. These interactions become even more complex understanding that each region in relationship to the core lesion demonstrates distinct mechanisms. The core region demonstrates progressive cavitation, while the peri-infarct tissue becomes increasingly plastic. There are also studies demonstrating that the contralateral cortex may have independent, temporal changes after ischemia, although these behavioral tests are limited (Cramer 2004, 2006b). Thus, understanding the complexities of these interacting systems as they develop after ischemia in a spatial manner is key to further elucidating the underlying mechanisms for future preventions and treatments. However, early ischemic and NRG-1 treatment induced spatial profiles of neuronal cells have yet to be characterized.

1.6 Neuregulin-1 and Clinical Progress NRG-1/Neucardin showed significant efficacy for improving cardiac function in multisite phase II patient studies (Gao 2010; Jabbour 2011). Systemic administration of recombinant human NRG-1/Neucardin was used in a multicenter phase II clinical trial investigating its efficacy and safety in patients with chronic heart failure in China and Australia. NRG-1/Neucardin was shown to be safe in patients and to have significant efficacy in improving cardiac function. Clinical trials have been initiated in the U.S. (ClinicalTrails.gov

identifiers NCT02664831; NCT01258387; NCT01251406) and phase III human clinical trials for heart failure in China. NRG-1/Neucardin has also shown a survival benefit in subjects with severe heart failure in the ongoing phase III study. The GMP manufacturing of NRG-1/Neucardin has been approved for use in Phase III clinical trials in the US by the Food and Drug Administration (FDA). NRG-1/Cimaglermin is the full-length extracellular domain of NRG-1β3 and has been used in clinical development for chronic heart failure (Lenihan 2016).

Overall, NRG-1 has demonstrated potential as a multiple mechanistic treatment for ischemic stroke targeting neuroprotective, anti-inflammatory, and neuroregenerative mechanisms on multiple neuronal cell types. However, further characterizing the mechanistic role of NRG-1 treatment in a spatiotemporal manner is crucial to progressing the understanding of its potential for success after ischemic stroke.

Chapter 2: Neuroprotection by Exogenous and Endogenous Neuregulin-1 in Mouse Models of Focal Ischemic Stroke

2.1 Introduction

In this study, we examined the neuroprotective efficacy of exogenous and endogenous NRG-1 on cerebral injury after the induction of ischemia by middle cerebral artery occlusion (MCAO) in mice. NRG-1 homozygous knockout mice are embryonic lethal at embryonic day 10.5. However, heterozygous knockout mice lacking one functional copy of the gene for NRG-1 (NRG-1+/−) express reduced levels of brain NRG-1 (Erickson 1997; Gerlai 2000; Sandrock 1997) and display hyperactive and schizophrenia-like phenotypes during neurobehavioral testing (O'Tuathaigh 2007, 2008, 2010; Stefansson 2002). We demonstrated that exogenously administered NRG-1-protected neurons from cerebral ischemia in both male and female mice. In addition, NRG-1+/− mice

displayed significantly larger infarcts than wild-type littermates, suggesting a neuroprotective role for endogenous NRG-1. Our data demonstrate that NRG-1 is a potent neuroprotectant against ischemic brain injury with high clinical potential. These findings may aid in identifying a novel therapeutic strategy for the treatment of stroke.

2.2 Materials and Methods

Animals All animals used in these studies were treated humanely and with regard for alleviation of suffering and pain, and all protocols involving animals were approved by the IACUC of Morehouse School of Medicine and University of California-Riverside prior to the initiation of experimentation. Male and female C57BL6 mice (8–10 weeks old) were purchased from Charles River (Wilmington, MA) and housed with a 12-h daily light/dark cycle. Male and female (10 months old) NRG-1 heterozygous transgenic mice (NRG-1+/−) and wild-type littermates (WT; NRG-1+/+) were also used in this study (Meyer 1995). The NRG-1 gene knockout mouse was generated by deletion of exons 7, 8, and 9, which encode the carboxy terminal of the EGF domain of all known NRG-1 isoforms. Mice with homozygous knockout of NRG-1 (NRG-1−/−) are embryonic lethal. However, the NRG-1+/− mice display reduced brain NRG-1 levels which are viable but display some abnormal neurobehavioral functions (Erickson 1997; Gerlai 2000; Sandrock 1997; Stefansson 2002). Food and water were provided ad libitum. All surgical procedures were performed by sterile/ aseptic techniques in accordance with institutional guidelines.

Transient Middle Cerebral Artery Occlusion Animals were subjected to left MCA occlusion (MCAO). Mice were anesthetized with 1.5% isoflurane in 68.5% N2O and 30% O2. MCA occlusion was induced by the intraluminal suture transient MCAO method as previously described (Barber 2004). The left common carotid artery (CCA) was exposed through a midline incision and

was carefully dissected free from surrounding nerves and fascia. The occipital artery branches of the external carotid artery (ECA) were then isolated, and the occipital artery and superior thyroid artery branches of the ECA were coagulated. The ECA was dissected further distally. The internal carotid artery (ICA) was isolated and carefully separated from the adjacent vagus nerve, and the pterygopalatine artery was ligated close to its origin with a 6–0 silk suture. Then, a 12-mm 7–0 surgical monofilament nylon suture with rubber silicon (Doccol, Sharon, MA) was inserted from the external carotid artery (ECA) into the internal carotid artery (ICA) then into the circle of Willis to occlude the origin of the left middle cerebral artery. The nylon suture was withdrawn 1 h following ischemia, and the brain tissues were reperfused for 23 h before sacrifice. Mice within the intravenous treatment group underwent filament occlusion for 90 minutes, and the brain tissues were reperfused for 22.5 h before sacrifice because of variability in baseline infarct size between male and female mice with 60 minutes of MCAO. Regional cerebral blood flow (CBF) was measured by continuous laser Doppler flowmetry (LDF) with a laser Doppler probe (Perimed, Kings Park, NY) placed in the ipsilateral skull close to the middle cerebral artery from the beginning of the MCAO surgery until 15 minutes after reperfusion. For NRG-1+/− (n = 6) and WT (n = 6) knockout mice, MCAO occurred for 45 minutes, and the brains were reperfused for 23.25 h before sacrifice. The 45-minute time point was chosen so that infarction was submaximal which allowed us to determine if infarcts grew larger in the transgenic animals. The surgical procedure was considered successful if CBF was reduced by ≥ 70% immediately after placement of the occluding suture; otherwise, mice were excluded.

To determine the effects of NRG-1 on ischemic stroke, mice were randomly divided into two treatment groups and injected intra-arterially (i.a.) with either a single-bolus 5-μL dose of vehicle (0.1% BSA in PBS) or NRG-1β (10 μmol/L NRG-1 (EGF-like domain, R&D Systems, Minneapolis, MN) in 1% BSA in PBS) through a Hamilton syringe as previously described (Xu

2004, 2005, 2006). This resulted in the administration of 16 μg of NRG-1/kg body weight. NRG-1 (n = 9) or vehicle (PBS; n = 9) was administered by bolus injection into the ICA through the ECA immediately before reperfusion. A second group of female (n = 6) and male (n = 4) mice were injected intravenously (i.v.) into the tail vein with either a single-bolus 100-μL dose of vehicle (0.1% BSA in PBS) or NRG-1β (100 μg/kg) with a 30-G needle immediately after filament insertion. All NRG-1 and vehicle treatment studies were performed in a blinded manner. Core body temperature was closely monitored with a rectal probe and maintained at 36.1 ± 0.1 °C with a Homeothermic Blanket Control Unit (Harvard Apparatus, Holliston,MA) during anesthesia to prevent hyperthermia as a confounding factor (Barber 2004).

Infarct Size Measurement and Neurobehavioral Testing Twenty-four hours after MCAO, 1.0- or 2.0-mm-thick brain sections were stained with 2–5% triphenyl tetrazolium chloride (TTC) solution and then transferred into a 4% formaldehyde solution for fixation. The infarcted region appears white, whereas the normal non-infarcted tissue appears red. The infarct area was identified by using five to seven slices of coronal sections from each brain. The infarct area was calculated in a blinded manner by capturing the images with a digital camera. Percentages of cortical and striatal infarct were calculated as a percentage of cortical and striatal volume, respectively (percentage of total infarct = infarct volume/(hemispheric volume) × 100%.). Infarct volumes were analyzed by t test; $p < 0.05$ was regarded as significant. Mice were assessed for neurobehavioral deficits 24 h after MCAO. The neurobehavioral score evaluation system is as follows: 0, normal; 1, consistent forelimb and axial flexion toward the contralateral to the lesion side when lifted by the tail; 2, observations of score 1 with consistently reduced resistance to lateral push and gait toward the paretic side; 3, observations of score 2 plus large or weak circling toward the paretic side; and 4, score 2 plus circling toward the paretic side (Barber 2004).

Histology and Immunohistochemistry After MCAO, mice were deeply anesthetized with 2% isoflurane and perfused transcardially with saline followed by cold 4% paraformaldehyde (PFA) solution in PBS for 30 minutes (n = 4–5 animals/ group). Brains were quickly removed and cryoprotected in 30% sucrose. The brains were then frozen in OCT compound and stored at – 80°C until sectioning. Coronal sections of 10–20-μm thickness were cryosectioned and mounted on slides which were then stored at − 80 °C until further processed. Fluoro Jade B (FJB; AG310, Millipore, Billerica, MA) labeling was performed according to the manufacturer's protocol with minor modifications. Briefly, after 30 minutes drying at 50 °C, sections were post-fixed with 4% paraformaldehyde for 15 minutes, washed with distilled water, and then directly incubated in 0.06% potassium permanganate (KMnO4) for 10 minutes on a shaker table followed by distilled water for 2 minutes. Sections were then incubated in a freshly prepared solution of 0.0004% FJB for 20 minutes, rinsed in distilled water, and then dried at 50 °C. Dried slides were cleared by immersion in xylene for 2 minutes before cover slipping with DPX mounting medium.

TUNEL labeling was performed using the in-situ death detection kit from Roche Molecular Biochemicals (Indianapolis, IN). Briefly, sections were incubated in 20 μg/ml proteinase K solution for 10 minutes at room temperature to increase permeability. After 2 washes in PBS, sections were immersed in the TUNEL reaction mixture, containing biotinylated dUTP and terminal deoxynucleotidyl transferase (TdT) conjugated with fluorochrome tetramethyl rhodamine red for 60 minutes at 37 °C in a dark, humidified atmosphere. The process was terminated by washing sections twice with a blocking buffer (PBS, 0.1% Triton X-100, and 5 mg/mL BSA). In each assay, negative controls were included using the same incubation procedure but omitting TdT in the process, whereas positive controls were performed by incubating the permeated sections with DNase (1 μg/mL) to induce DNA strand breakage.

For immunohistochemical studies, sections were dried at room temperature for 30 minutes. After rinsing with 0.01M PBS, sections were blocked in PBS containing 5% normal goat serum and 0.3% Triton X-100 for 1 h at 4 °C and then incubated overnight at 37 °C with primary antibodies of monoclonal mouse anti-NeuN (1:200, MAB314, Millipore, Billerica, MA). Sections were washed with PBS and incubated with a FITC-conjugated goat anti-mouse IgG antibody (1:400, Cat#115-095-146, Jackson ImmunoResearch Laboratory, West Grove, PA) for 1 h at room temperature. A Zeiss microscope equipped with a CCD camera (Carl Zeiss Microimaging Inc., Thornwood, NY) was used to capture all digital images of sections at ×20 magnification.

Quantification FJB- and NeuN-Immunopositive Cells The number of FJB- and NeuN-positive cells was determined using Image Pro Plus and ImageJ software (Media Cybernetics, Inc., Bethesda, MD) by an individual who was blinded to the experimental treatments. Only normal morphological profiles of NeuN-positive cells were counted, and shrunken NeuN-positive signals were excluded. A mean value of FJB-positive or NeuN cells per unit area from five brain sections within the brain regions was obtained for each individual mouse brain. Data were expressed as mean ± SEM. These mean values from each individual mouse were used as the statistical unit of measure for analysis by t test to determine statistically significant treatment effects.

2.3 Results

NRG-1 Protects Against Ischemia-Induced Brain Injury We examined the neuroprotective effects of NRG-1 following MCAO in mice. NRG-1 was administered immediately after reperfusion. Brain tissues were analyzed in mice treated with NRG-1 or vehicle i.a. immediately after reperfusion and sacrificed 24 h after MCAO. Figure 2.1a illustrates a typical TTC staining of

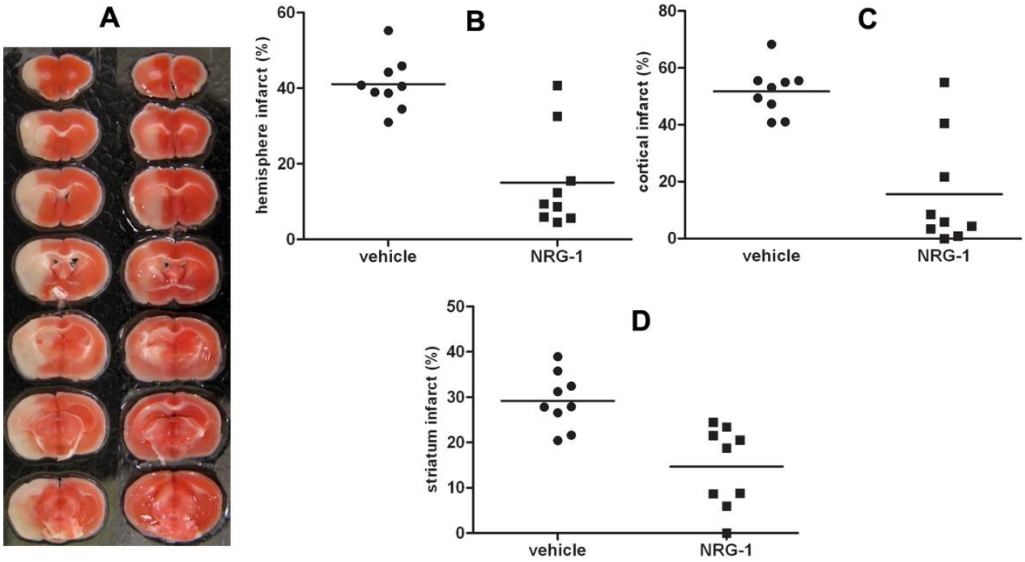

Figure 2.1 Neuroprotection with intra-arterial NRG-1 treatment shown by TTC. NRG-1 reduced infarct volume following MCAO/reperfusion. Mice were treated with NRG-1 (16 μg/kg) or vehicle immediately after MCAO followed by 23 h of reperfusion. Brains were removed, sliced into seven coronal sections (1 mm thick), and treated with 2% TTC (a). NRG-1 reduced total infarct volume by 67% (b; $p < 0.0001$). Treatment with NRG-1 resulted in a 72% reduction in cortical infarct size (c; $p < 0.0001$) and 50% in subcortical regions (d; $p = 0.001$). N = 9 mice per treatment group

brain sections treated with vehicle or NRG-1 after MCAO. Compared with controls, i.a. administration of NRG-1 drastically reduced infarct volume after MCAO in mice as we and others previously showed in rats (Guo 2006; Li 2007; Shyu 2004; Wang 2015, 2018; Xu 2004, 2005, 2006). The percentage of total infarct volume to the ipsilateral hemisphere in vehicle-treated animals was 41%. NRG-1 significantly reduced the total infarct volume to 15% of hemispheric volume representing a 67% reduction in infarct size (from 78.9 to 25.6 mm3) (Figure 2.1b). The relative reduction in cortical and subcortical neuronal injury was also calculated. The infarct volume of control animals represented 56%of the total size of the ipsilateral cortex. Treatment with NRG-1 resulted in an infarct that was reduced to 16% of the ipsilateral cortex, which corresponds to a 72% reduction in cortical infarct size (from 53.0 to 15.0 mm3) (Figure 2.1c). NRG-1 treatment reduced infarction by 50% in subcortical regions (Figure 2.1d). Regional CBF was measured by LDF for each mouse during MCAO and after reperfusion. NRG-1 did not significantly affect the CBF reduction after MCAO ($p = 0.8695$) or recovery after reperfusion ($p = 0.8722$) (Figure 2.2; n

= 9 in each group). NRG-1 also did not affect the baseline body temperature, body temperature 24 h post-MCAO, or body weight loss (Figure 2.3). No significant difference in neurological outcome was observed between controls and NRG-1-treated animals at this time point (data not shown).

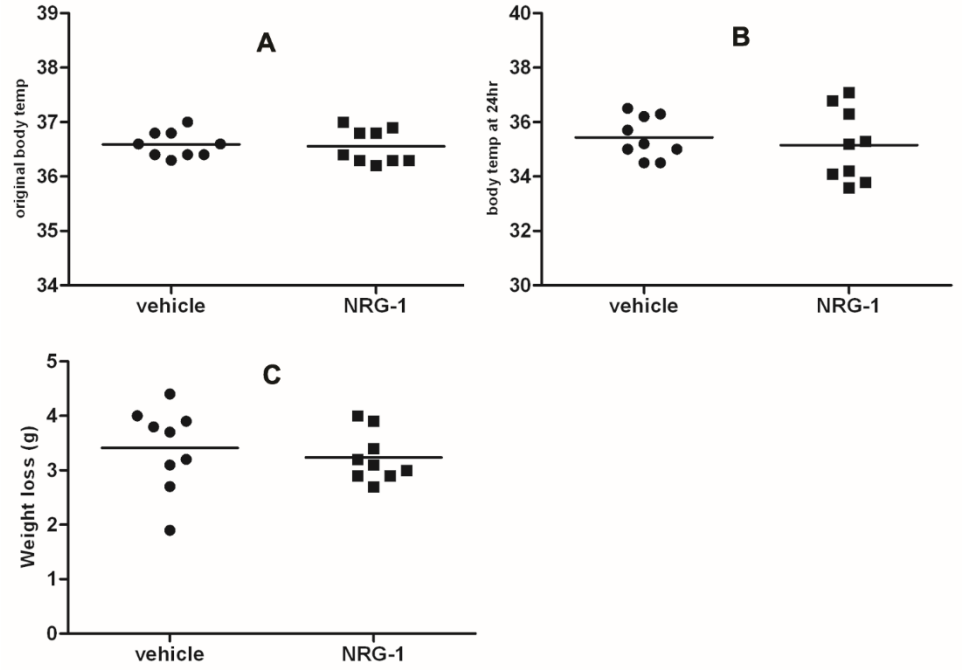

Figure 2.2 NRG-1 does not affect regional CBF after MCAO. Regional CBF was measured by LDF for each mouse during MCAO and after reperfusion. NRG-1 did not significantly affect the CBF reduction after MCAO (a; p = 0.8695) or recovery after reperfusion (b; p = 0.8722) (n = 9 in each group).

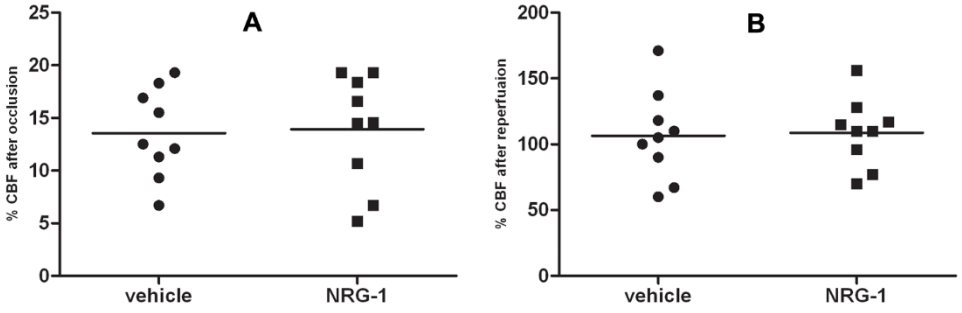

Figure 2.3 NRG-1 does not affect animal body temperature or weight after MCAO. NRG-1 or vehicle was administered immediately after reperfusion. There was no statistical significance between vehicle and NRG-1-treated animals for the baseline body temperature (a; p = 0.8020); body temperature 24 h post-MCAO (b; p = 0.5944), or body weight loss (c; p = 0.5584) (n = 9 in each group).

NRG-1 Blocks Ischemia-Induced Neuronal Death Neuronal injury and the neuroprotective effects of NRG-1 treatment were also assessed by FJB staining. Brain tissues from mice treated with either NRG-1 or vehicle were examined 24 h after MCAO/reperfusion, and extensive FJB staining was found within the ischemic cortical and subcortical regions (Figure 2.4). Ischemia-induced FJB staining was reduced by 64% NRG-1 treatment in the areas within the cerebral cortex. NRG-1 also dramatically reduced TUNEL labeling after MCAO (Figure 2.5). MCAO reduced NeuN immunoreactivity in cortical neurons (Figure 2.6). These injured areas showed high numbers of FJB labeling in adjacent sections as seen in Figure 2.4. Neighboring neurons that were not injured

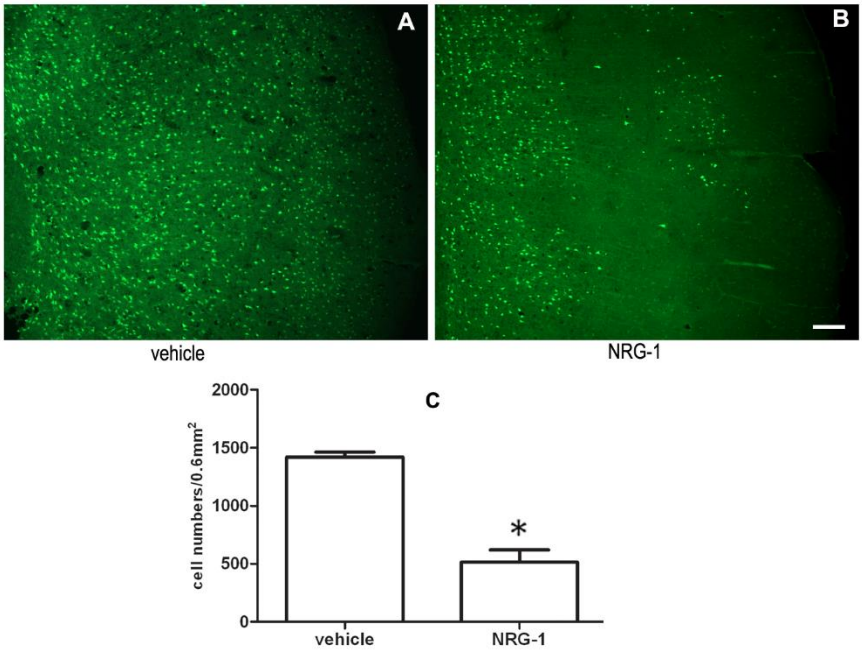

Figure 2.4 NRG-1 reduced FJB staining in the brain following MCAO/reperfusion. Brains from mice treated with either vehicle or NRG-1 were examined 24 h after MCAO/reperfusion. Extensive FJB staining was found in brain tissues following ischemia (a). Ischemia-induced FJB staining was significantly reduced by NRG-1 (b). A mean value of FJB positive or per unit area from five brain sections within the brain regions was obtained for each individual mouse brain (c; p = 0.0001). Data are expressed as mean ± SEM. Scale bar = 100 µm.

showed relatively higher levels of NeuN immunoreactivity. NRG-1 post-treatment rescued NeuN immunoreactivity following MCAO.

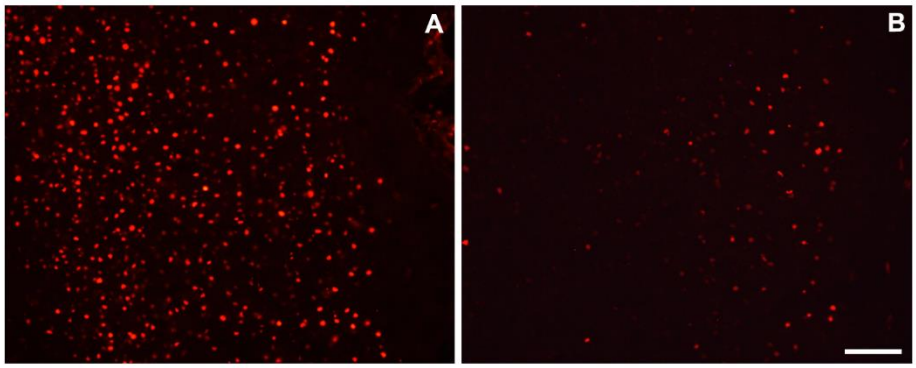

Figure 2.5 NRG-1 blocks ischemia induced apoptosis. Brains from mice treated with either vehicle or NRG-1 were examined 24 h after MCAO/reperfusion using TUNEL labeling. Extensive TUNEL labeling was found within the brain following ischemia (a). Ischemia-induced TUNEL labeling was blocked by NRG-1 treatment in the areas within the cerebral cortex (b). Scale bar = 50 µm.

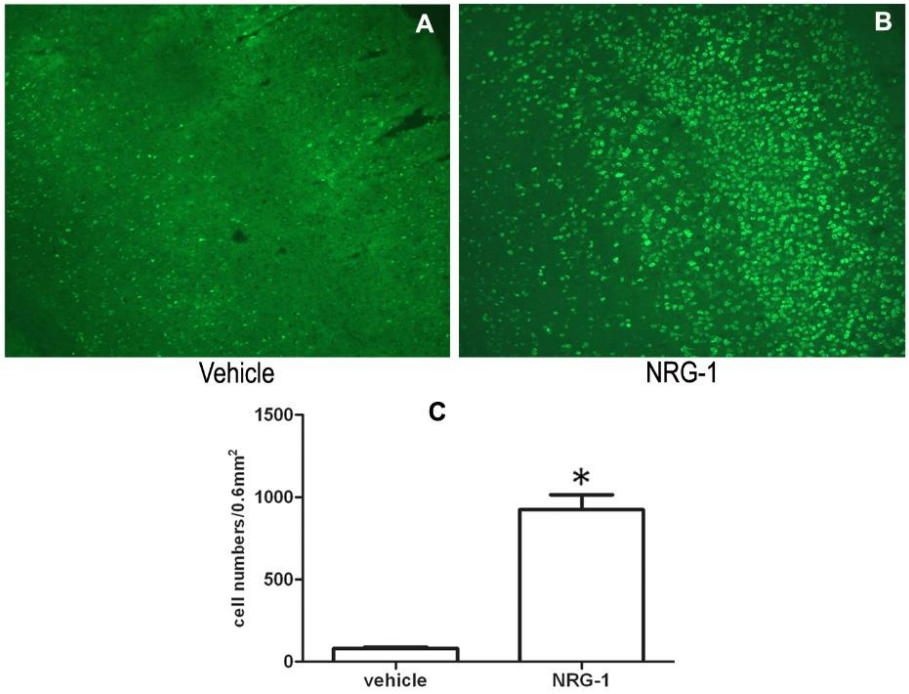

Figure 2.6 NRG-1 protects neurons from ischemic damage following MCAO/reperfusion. MCAO/reperfusion resulted in reduced NeuN immunoreactivity in cortical neurons (a). NRG-1 treatment rescued NeuN immunoreactivity (b, c; p = 0.0001). Scale bar = 100 µm

Neuroprotection was observed following i.v. administration of NRG-1 in male and female mice (Figure 2.7a, b). Vehicle-treated mice exhibited an average total infarct volume of 24.9% and NRG-1 reduced that percentage to 13.3%, a 46.6% reduction (Figure 2.7c; 2 males + 3 females per treatment group). Vehicle-treated mice resulted in an average cortical infarct volume of 26.8% that NRG-1 significantly reduced to an average of 7.5%, a 72.1% reduction specifically within the ipsilateral cortex. No difference in lesion size was seen within the ipsilateral subcortical region.

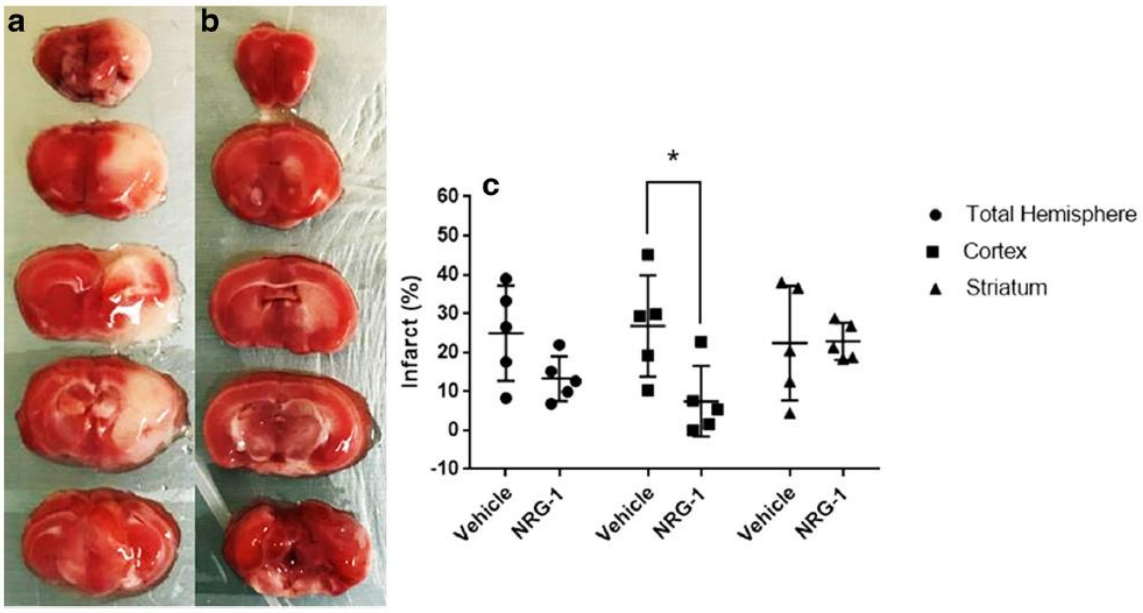

Figure 2.7 NRG-1 reduced infarct volume via intravenous administration in male and female mice. a Vehicle or b NRG-1 (100 μg/kg) was administered immediately after filament insertion. MCAO occurred for 90 minutes followed by 23 h of reperfusion. Brains were removed, sliced into five coronal sections (2 mm thick), and treated with 2% TTC. c NRG-1 reduced total infarct volume by 46.6% (b; $p < 0.05$). Treatment with NRG-1 resulted in a 72.1% reduction in cortical infarct size (c; $p < 0.05$) and no significant difference in subcortical regions. N = 5 mice (2 males + 3 females) per treatment group.

Endogenous NRG-1 Protects Neurons from Ischemic Injury To determine if endogenous NRG-1 is involved in ischemic brain injury, we examined cerebral infarction in male and female (3 males and 3 females per group) NRG-1+/− mice and WT littermates. MCAO was performed for 45 min rather than 1 h to produce smaller, submaximal infarcts and examine whether reduced endogenous

NRG-1 could result in increased neuronal damage. There was no difference in CBF reductions and recovery between WT and NRG-1+/− mice (Figure 2.8a, b); however, the infarct volume in the cerebral cortex of NRG-1+/− mice was sixfold larger than that observed in WT mice (Figure 2.8c–f). However, there was no difference in subcortical infarct volume between the two groups and thus total hemisphere infarct volume was not statistically significant when compared.

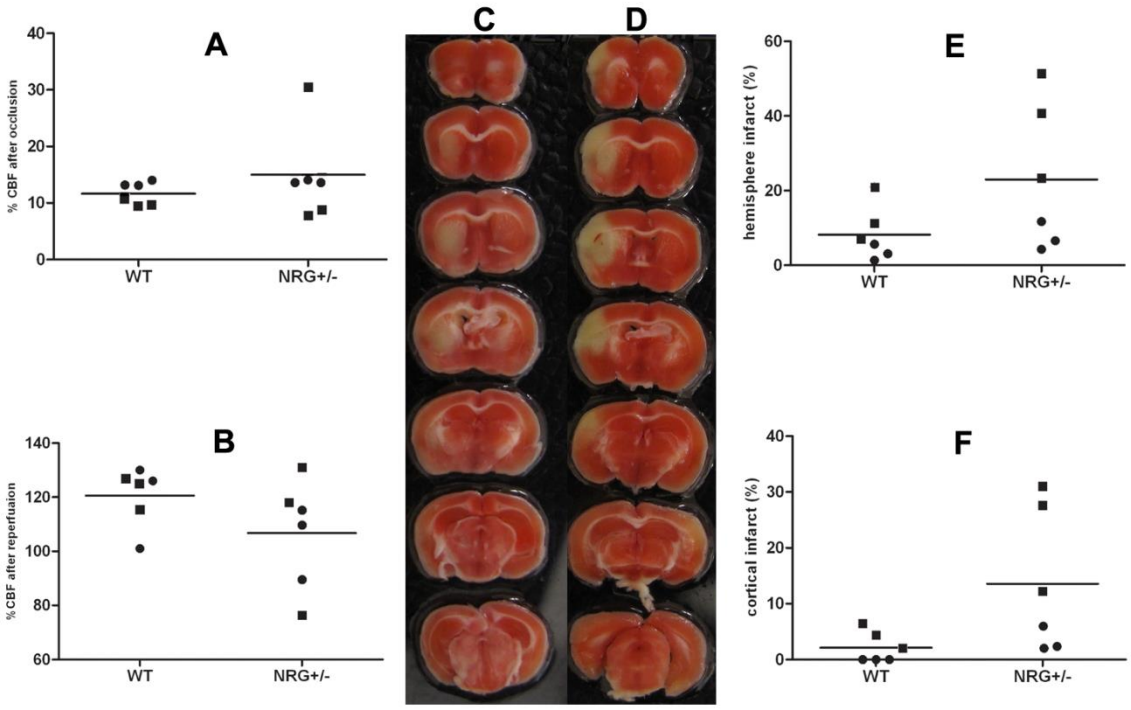

Figure 2.8 Endogenous NRG-1 protects neurons following MCAO/reperfusion. NRG-1+/− mice and WT littermates were subjected to 45 minutes MCAO followed by 23.25 h of reperfusion. There was no difference in CBF reduction (a, p = 0.3494) or recovery (b, p = 0.1645) between WT and NRG+/− mice. TTC labeling was used to measure brain infarction in WT (c) and NRG-1+/− mice (d). There was no difference in subcortical infarct volume between the two groups (not shown), and thus, total hemisphere infarct volume was not statistically significant when compared (e; p = 0.0549). However, the infarct volume in the cerebral cortex of NRG-1+/− mice was 6-fold larger than that observed in WT mice (f; p = 0.0406) N = 6 per experimental group.

2.4 Discussion

NRG-1 belongs to a family of multipotent neuroprotective and anti-inflammatory growth factors that include acetylcholine receptor–inducing activities (ARIAs), glial growth factors (GGFs), heregulins, and neu differentiation factors (NDFs) (Falls 1993; Ho 1995; Holmes 1992; Marchionni 1993;Wen 1992).We have shown that NRG-1 reduced ischemic brain injury when administered either before or 13.5 h after MCAO (Xu 2006). NRG-1 has also been shown to promote functional recovery in a rat stroke model when administered intravenously up to 7 days after ischemia (Iaci 2010). In this study, we examined if exogenously applied or endogenous NRG-1 was neuroprotective in a mouse MCAO model. We observed that both i.a. and i.v. administration of NRG-1 reduced neuronal injury in mice. The neurobehavioral test we used to examine the acute effects of ischemic stroke and NRG-1 did not correlate with the histological protection as we observed in the rat stroke model (Xu 2004, 2006). Future studies will employ more sensitive tests to examine the long-term neurobehavioral consequences of NRG-1 treatment following ischemia in mice beyond the 24-h time point.

We also observed that ischemic brain injury was more severe in NRG-1+/− knockout mice compared with WT mice suggesting that endogenously expressed NRG-1 is involved in the function of neurons under normal conditions. NRG-1−/− homozygous knockout mice die in utero, but heterozygous NRG-1+/− mice are viable and with reduced amounts of NRG-1 in the brain (Erickson 1997; Gerlai 2000; Sandrock 1997; Stefansson 2002). Heterozygous NRG-1 knockout mice were shown to have a “schizophrenia-like” phenotype including alterations in prepulse inhibition and anxiety-like behaviors (Erickson 1997; Gerlai 2000; O'Tuathaigh 2007, 2008, 2010; Sandrock 1997; Stefansson 2002). Polymorphisms in the NRG-1 gene have also been associated with increased risk for schizophrenia in human patients (Stefansson 2002, 2004). Similar results were shown with erbB4 knockout mice following stroke. Neuroprotection by NRG-1 against

cerebral ischemia was prevented in the mice with erbB4 deleted in parvalbumin (PV)-positive interneurons (Guan 2015).

An important finding in this study is that NRG-1 was neuroprotective in both male and female mice. Pre-menopausal women are protected from ischemic stroke compared with males (Murphy 2004). However, this neuroprotective capacity is lost in post-menopausal women, where estrogen levels reduced. Experimental studies have shown that premenopausal female rodents and non-human primates were protected from ischemia-induced brain injury compared with males (Alkayed 1998; Murphy 2004, 2008; Toung 2004). The observation that the neuroprotective effect of NRG-1 was gender-independent makes it a more attractive clinical candidate for neuroprotective therapy.

The STAIR report produced in response to the multiple failed stroke neuroprotection clinical trials suggested that pre-clinical stroke studies be performed in multiple species. Therefore, it is clinically significant that NRG-1 is equally neuroprotective in both mice and rats. Recently, we developed a novel, minimally invasive ischemic stroke model with young male rhesus macaques (Rodriguez-Mercado 2012) which has been replicated with similar results in aged female monkeys (Zhang 2015; Li 2018). This procedure reliably produced infarcts and resulted in discrete and limited neurobehavioral deficits, indicating the potential of this stroke model for chronic neuroprotection studies in the future. Therefore, in future studies we will be able to directly examine the neuroprotective capacity of NRG-1 following stroke in males and female non-human primate stroke models.

Thrombolysis is the only approved therapy for acute ischemic stroke and can only be used in a limited patient population. The present study demonstrates that NRG-1 is a viable candidate neuroprotectant to treat acute ischemic stroke. NRG-1 (Neucardin; Zensun Biotechnology, Shanghai, China) is currently in phase III human clinical trials for the treatment of heart failure and

showed significant efficacy for improving cardiac function in phase II patient studies in China (Chinese Clinical Trial: ChiCTR-TRC-00000414) and Australia (Australian New Zealand Clinical Trials Registry: ACTRN12607000330448). Three additional clinical trials to determine the ability of NRG-1 to improve cardiac function after heart failure have been initiated in the USA (ClinicalTrials.gov identifiers NCT01258387; NCT01541202; NCT01251406). These clinical studies demonstrated that NRG-1 significantly improved heart function in patients and the effective doses were shown to be safe and tolerable (Gao 2010; Jabbour 2011). This suggests rationale for future clinical adjunctive treatment with NRG-1 and tPA or endovascular thrombectomy. We recently developed a partnership with Zensun to pursue FDA approval to use Neucardin in clinical trials for stroke treatment (https://news.ucr.edu/articles/2019/05/09/hope-horizon-treatingstroke).

Recent studies showed that erbB4 prevented neuronal injury and improved blood-brain barrier integrity in animal models of subarachnoid hemorrhage (Qian 2018; Yan 2017). This suggests that NRG-1 would not induce hemorrhagic transformation after ischemia and could protect patients from tPA-mediated toxicity. These findings could support the development of clinical studies using NRG-1 alone or in conjunction with other therapies for the treatment of patients with acute ischemic stroke.

Chapter 3: Spatial Analysis of Neural Cell Proteomic Profiles following Ischemic Stroke in Mice using High-Plex Digital Spatial Profiling

3.1 Introduction

In this study, we examined the spatial regulation of protein profiles initiated by ischemia. By utilizing immunohistochemistry and Nanostring Digital Spatial Profiling (DSP) we analyzed panels of proteins in regions of interest including the ischemic core border, peri-infarct, and PiNT

at 3- days post-ischemia compared to regions in the contralateral cortex. NanoString's GeoMx DSP technology generates profiling data for validated protein analytes using high-plex spatial profiling to rapidly and quantitatively assess the biological implications of the heterogeneity within the tissue samples. We demonstrated that the ipsilateral hemisphere particularly initiated distinct proteomic regulatory profiles in a spatial manner that can be co-localized consistently with the cellular markers, fluoro Jade B (FJB), GFAP, and Iba-1. Additionally, the core border region presented a unique proteomic profile that represents neuronal death, apoptosis, immunoreactivity, and early degeneration. Most notably, the core border resulted in a decrease of the neuronal proteins Map2 and NeuN, an increase in the autophagic proteins BAG3 and CTSD, an increase in the microglial and peripheral immune invasion proteins Iba1, CD45, CD11b, and CD39, and an increase in the neurodegenerative proteins BACE1, APP, αβ 1-42, ApoE, and hyperphosphorylated tau protein S-199. The peri-infarct region demonstrated increased astrocytic immunoreactivity, apoptotic, and neurodegenerative proteomic profile, with an increase in the autophagic protein BAG3, GFAP, and hyperphosphorylated tau protein S-199. The PiNT region displayed minimal changes compared to the contralateral cortex with only an increase in GFAP. These findings may aid in identifying a novel therapeutic strategy for the treatment of stroke.

3.2 Materials and Methods

Animals All animals used in these studies were treated humanely and with regard for alleviation of suffering and pain, and all protocols involving animals were approved by the IACUC of University of California-Riverside prior to the initiation of experimentation. Male and female C57BL6 mice (8–10 weeks old) were purchased from Jackson Laboratories (Bar Harbor, Maine) and housed with a 12-hour daily light/dark cycle. Food and water were provided ad libitum. All

surgical procedures were performed by sterile/aseptic techniques in accordance with institutional guidelines.

Photothrombotic Middle Cerebral Occlusion Animals were subjected to left photothrombotic MCA occlusion (MCAO). Mice were anesthetized with 2% isoflurane and circulating air (N2O:O2 at approximately 2:1) and maintained anesthetized during the procedure via a modified gas tubing nose connection on a stereotaxic instrument. Eye lubricant was applied to protect the eyes and body temperature was maintained via a heating pad placed underneath the mice during surgery at 37°C. MCAO was performed in an adapted accordance to Zhong et al. (Zhong 2010). Rose Bengal (10 mg/mL; Cat#330000, Sigma, Burlington, MA) was injected intraperitoneally (i.p.) at 10 mL/g and allowed to incubate for 8 minutes. The animal was stabilized in the stereotaxic instrument and the scalp hair was removed. The scalp was disinfected with iodine and ethanol, then followed by a midline skin incision to expose the skull above the left sensorimotor cortex. A 2-mm diameter focal green laser (520nm; Cat# LP520-MF100 ThorLabs Inc, Newton, NJ) was directed at 2-mm lateral left and 0.6-mm posterior of bregma. Laser irradiation occurred for 20 minutes at 10 mW. After irradiation, the midline incision was sealed with Vetbond glue followed by triple antibiotic ointment. Mice were then placed into a 37°C incubation chamber for 20-30 minutes to recover. Sham control animals included two groups: 1) Rose Bengal injection without laser irradiation and 2) laser irradiation without Rose Bengal injection. Mice were sacrificed at 3 days post-ischemia (dpi).

Histology and Immunohistochemistry After MCAO, mice were deeply anesthetized with 2% isoflurane and perfused transcardially with saline followed by cold 4% paraformaldehyde (PFA) solution. Brains were quickly removed and maintained in 4% PFA for 24 hours. Brains in preparation for histological and immunohistochemical analysis were quickly removed after transcardial perfusion and maintained in 4% PFA for 24 hours before being cryoprotected in 30%

sucrose. The brains were then flash frozen and stored at – 80°C until sectioning. Coronal sections of 12–15 μm thickness were cryosectioned and mounted on slides which were then stored at −80°C until further processed.

Cresyl violet (Cat#C5042, Millipore, Billerica, MA) stain was first reconstituted from powder with distilled water, allowed to stir overnight, and then 0.3% glacial acetic acid was added and mixed thoroughly. Sections were stained with cresyl violet on slides beginning with rehydrating steps of 15 minutes incubation with 95% ethanol, 1 minute with 70% ethanol, 1 minute with 50% ethanol, 2 minutes with distilled water, and 1 minute with distilled water. Sections were then stained with cresyl violet warmed to 37.5°C for 3 minutes followed by distilled water for 1 minute. Sections were then dehydrated with 1 minute of 50% ethanol, 2 minutes of 70% ethanol with 1% glacial acetic acid, 2 minutes of 95% ethanol, and 1 minute of 100% ethanol. After allowing the ethanol to dry off the sections, they were incubated with warmed cresyl violet again for 2 minutes followed by distilled water for 2 minutes. Sections were cleared with a 5-minute wash of Histoclear and mounted and cover slipped with DPX (Cat#06522, Millipore, Billerica, MA).

Fluoro Jade B (FJB; Cat#AG310, Millipore, Billerica, MA) labeling was performed in an adapted accordance to Noll et al. 2019 to ensure infarct presence and record infarct size and location (Noll 2019). Sections were post-fixed with 10% formalin for 10 minutes and then washed twice with PBS for 5 minutes. Sections were then directly incubated in 0.06% potassium permanganate ($KMnO_4$) for 3 minutes followed by distilled water for 2 minutes. Sections were then incubated in a freshly prepared solution of 0.0004% FJB with DAPI for 20 minutes, rinsed in distilled water 3 times for 2 minutes, and then dried at 50°C.

For immunohistochemical studies, sections were dried at room temperature for 30 minutes. After rinsing with 0.01M PBS, sections were blocked in PBS containing 5% normal donkey serum

and 0.1% Triton X-100 for 1-2 hours at room temperature, rinsed with PBS/0.2% Tween-20 (PBST) and then incubated overnight at 4°C with primary antibodies of polyclonal rabbit anti-Iba-1 (1:1000, Cat#019-19741, Wako, Osaka, Japan) and Cy3-conjugated monoclonal mouse anti-GFAP (1:400, Cat#C9205, Sigma, Burlington, MA). Sections were washed 3 times with PBST, incubated with respective AlexaFluor594-conjugated donkey anti-rabbit IgG antibody (1:400, Cat#711-585-152, Jackson ImmunoResearch Laboratory, West Grove, PA) for 1 hour at room temperature, then rinsed 4 times with PBST before mounting with DAPI-Fluoromount-G (Cat#OB010020, Fisher Scientific, Pittsburgh, PA).

Immunohistochemical Quantification A Leica MZ FL III stereo microscope with a tethered dSLR camera was used to capture all digital images of cresyl violet stained sections. A Leica DM5500 B Automated Upright fluorescence microscope was used to capture all digital images of FJB stained sections at x5 magnification. A Nikon TS2-S-SM inverted fluorescence microscope equipped with a CCD camera was used to capture all digital images of sections at ×10 magnification. Cresyl violet images were captured to demonstrate photothrombotic damage at each investigated stereotaxic location (bregma +2, +1, and 0) and each investigated region of interest (ROI) with highlighted focus on the core border region (Figure 3.1).

Immunohistology images of FJB+ cells were captured at bregma +2 and +1 at 5x magnification to capture the entire image area of FJB+ cells. Images were taken at the ipsilateral core and corresponding contralateral cortical region of three separate tissue sections for each mouse. FJB+ cells were counted semi-automatically with ImageJ software (Media Cybernetics,

Inc., Bethesda, MD) after threshold at size 10-infinity (pixel units) and circularity 0.4-1.00. FJB+ cell counts were averaged for each stereotaxic location.

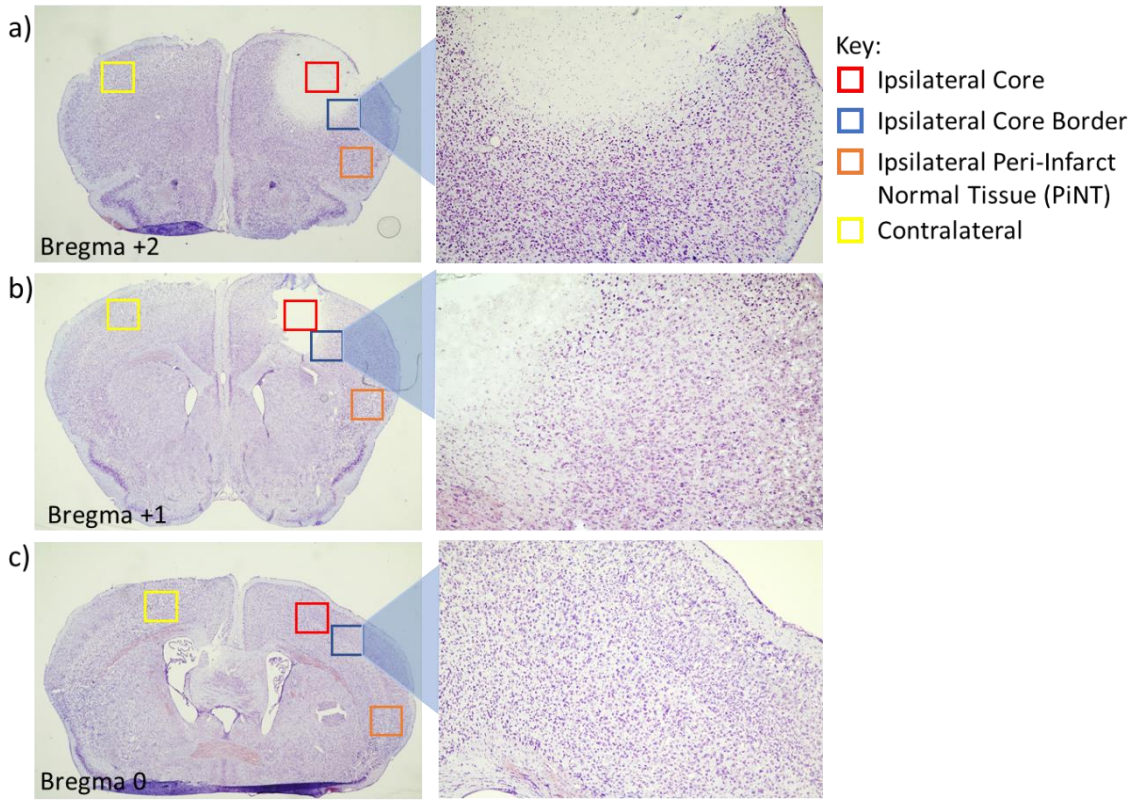

Figure 3.1 Representative Stereotaxic Locations and Regions of Interest at 3-days post-Ischemia. Coronal sections of mice with induced photothrombotic MCAO were stained with cresyl violet at 3 days after MCAO and examined qualitatively at bregma +2 (a) bregma +1 (b) and bregma 0 (c) with four ROIs: Ipsilateral core (red), Ipsilateral core border (blue), Ipsilateral Peri-Infarct Normal Tissue (PiNT; orange), and Contralateral (yellow) with higher magnification of the core border region. Infarct at 3-days post-ischemia demonstrated larger core damage at bregma +2 with some sustained damage at bregma +1, but no indicated damage at bregma 0. Core border region demonstrates a small increase in cell numbers at both bregma +2 and +1.

Immunohistology images of Iba-1, and GFAP were captured at approximately bregma +2, +1, and 0 at four different regions of interest: the core, core border, PiNT and contralateral cortex in three separate corresponding tissue sections for each mouse. Mean gray values were calculated with ImageJ software. All picture properties were obtained and ensured for consistency. Pictures were converted to 32-bit gray before analysis, and pictures were not altered in any other way. Area fraction was utilized as a control where all picture values must have 100% area fraction. Mean gray

value regions of interest technical replicates were averaged and were calculated as fold changes against the contralateral side. Iba-1 maxima count was analyzed with prominence=15, in areas of high tissue damage (based on cresyl violet staining) where background signal may be higher, prominence was increased to 18. Maxima count ROI technical replicates were averaged and calculated as fold changes against the contralateral side. Sham and MCAO groups fold-change mean gray values were compared using Student's two sample t-tests assuming unequal variances.

Formalin-Fixed Paraffin Embedded Tissue Preparation Brains in preparation for Nanostring DSP were continually dehydrated in preparation for paraffin embedding: 24 hours of 4% PFA was followed by 24 hours each in 40% ethanol, 70% ethanol, and a second change of 70% ethanol. Brains were then placed whole into cassettes and processed in a Tissue-Tek Processor in a 12-hour cycle (Table 3.1) before embedding coronally in paraffin.

Table 3.1 Tissue-Tek Processing Protocol

Reagent	**Time**
Ethanol	30 minutes
Ethanol	5 x 1 hour
CitriSolv	3 x 45 minutes
Wax	3 x 1 hour

Formalin-fixed, paraffin-embedded (FFPE) samples were sectioned to approximately bregma +2 and 5-μm thickness sections were mounted onto slides and allowed to dry at room temperature overnight. FJB labeling was performed as described above to ensure infarct presence and record infarct size and location. Samples confirmed with FJB+ cells indicating successful MCAO were sent to Nanostring (Seattle, WA) for slide mounting and GeoMx DSP profiling.

Nanostring Digital Spatial Profiling Analysis To visualize whole tissue, mounted slides were stained with oligo-conjugated antibodies for MAP2, Iba-1 and GFAP, and with Syto13 (nuclei) in the GeoMx DSP instrument. Circular geometric patterns (200 μm diameter) were used to identify

six ROIs on the scanned tissues of each sample: core border, peri-infarct, and PiNT regions on ipsilateral and contralateral hemispheres. The GeoMx Neural Cell Profiling protein panel (73 proteins) was utilized for this analysis. UV-cleavable oligo-conjugated antibodies according to the panel were dispensed onto each ROI, UV-cleaved off, aspirated into a plate, hybridized and counted by the GeoMx DSP instrument. All resulting spatial, quantified analysis was performed in the Nanostring GeoMx DSP analysis software. Background correction was determined by protein target correlation plot and high correlation was seen between Rb IgG, Rb IgGa, and Rb IgGb. All three IgG proteins were used for panel background correction via signal-to-background ratio. Spatial ROIs were compared using a linear mixed model (LMM) with Bonferroni-Hochberg (BH) correction and random effect for Scan ID and ROI ID. Fold changes were identified by comparing the ROI/contralateral ROI with a significance of p value <0.05.

3.3 Results

FluoroJadeB Identifies Ischemic Infarct 3 Days Post-MCAO We examined the consistency and ability to define the photothrombotic infarct at three days post-injury with the neurodegeneration stain, FJB. Brain tissues from mice with induced MCAO were sacrificed and examined spatially at three days after ischemia at bregma +2 and +1. Detectable FJB+ cells were found consistently throughout the infarct core at bregma +2, but not at bregma +1 (Figure 3.2). MCAO brain tissue exhibited a mean of 547.3 ± 114 FJB+ cells at bregma +2 with only a mean of 11.6 ± 19 at bregma +1. This demonstrated that neurodegenerative damage occurs and is detectable by FJB staining three days after MCAO with primary neuronal damage located at bregma +2.

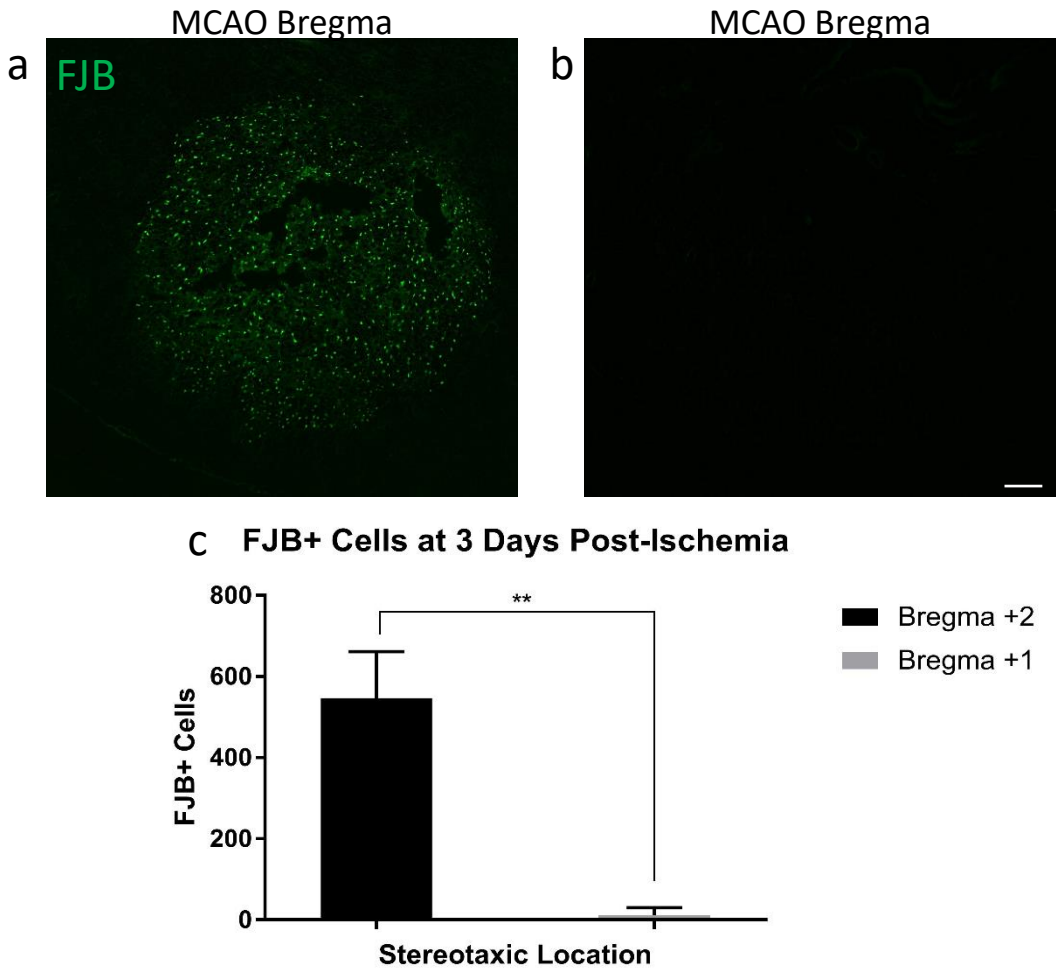

Figure 3.2 Neuronal Damage 3 Days Post-Ischemia. Brains from mice with induced MCAO were examined 3 days after ischemia. FJB+ cells were counted at bregma +2 and +1 at 5x magnification for whole infarct comparison. Extensive FJB+ staining was found at bregma +2 (a) but were not detected at bregma +1 (b). A mean value of FJB+ cells from three brain sections from each location was obtained for each individual mouse brain (c; $p<0.01$, n=4). Data are expressed as mean ± SD. Scale bar = 100 µm.

GFAP Increases in Core Border 3 Days Post-Ischemia To characterize the early inflammatory processes that occur after MCAO, astrocytic immunoreactivity was assessed in a spatial manner with the immunohistology marker, GFAP. Brain tissues from mice with induced MCAO and sham controls (SHAM) were sacrificed and examined at three days after ischemia at stereotaxic locations bregma +2, +1, and 0 within the ipsilateral core, core border, and PiNT for GFAP expression. High GFAP expression is not typically observed in the naïve or SHAM mouse cortex but is upregulated

within proliferating and activated astrocytes following neuronal injury (Davies 1998; Savchenko 2000; Nowicka 2008). Therefore, GFAP expression was analyzed as mean gray value fold change against the contralateral side to detect regional changes in GFAP expression. GFAP regional fold change expression in MCAO animals was compared to SHAM animals (Figure 3.3). GFAP expression significantly increased within the ipsilateral core border at both bregma +2 and +1 with a fold change of 1.76 ± 0.3 and 1.66 ± 0.29, respectively. No significant changes in GFAP mean gray value fold changes between MCAO and SHAM were seen in ipsilateral core or PiNT regions at any stereotaxic location. Additionally, GFAP mean gray fold change expression was non-distinct from SHAM at bregma 0 for all three regions. GFAP expression suggests that there is an increase in astrocytic inflammatory activity along the core border in a spatial manner at three days post-ischemia.

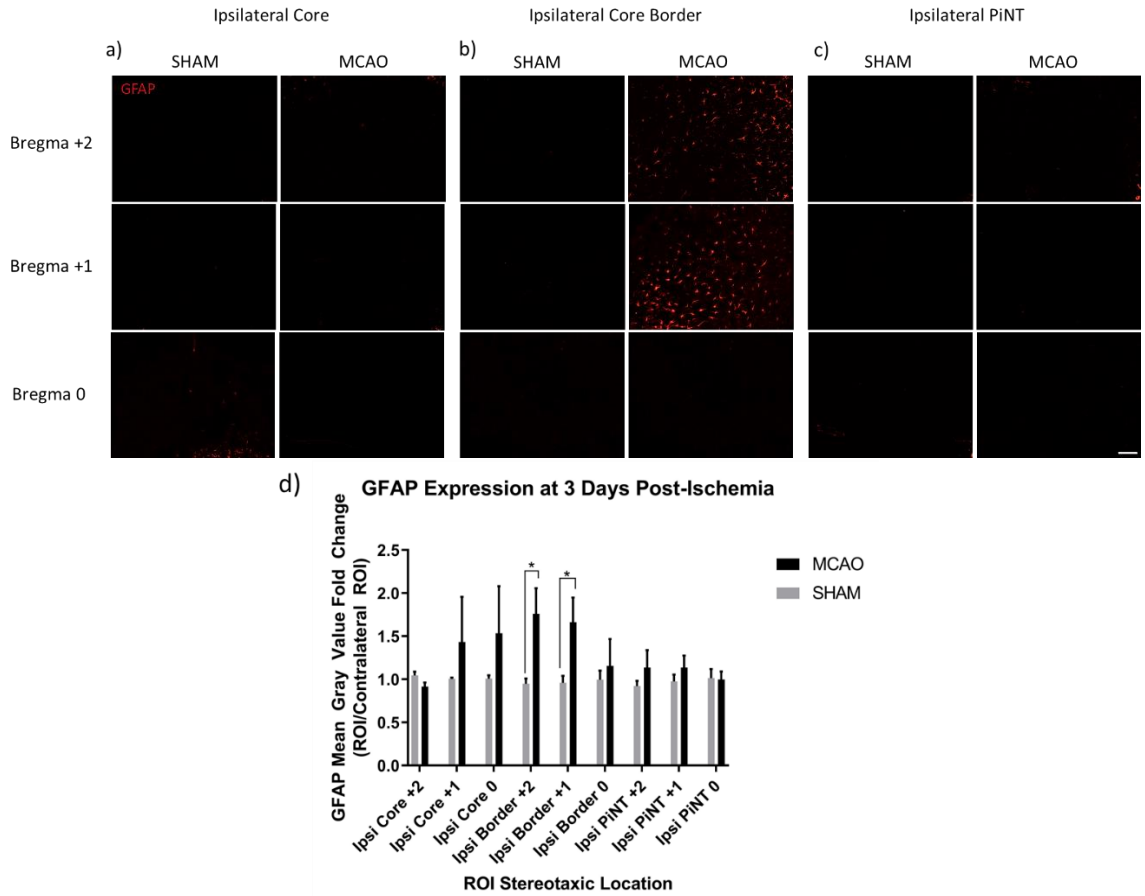

Figure 3.3 GFAP Expression Increases in Core Border 3 Days Post-Ischemia. Brains from mice with induced photothrombotic MCAO were examined spatially 3 days after MCAO for GFAP expression. Mean gray value fold change of GFAP expression compared to the contralateral hemisphere in the ipsilateral core (a) ipsilateral core border (b) ipsilateral PiNT (c). Mean gray value fold change increased significantly in the core border at bregma +2 and bregma +1 but was non-significant in bregma 0 (d). Mean gray value fold change of GFAP was non-significant in ipsilateral core or PiNT in any stereotaxic location. Data are expressed as mean ± SD; $p<0.05$, MCAO (n=4) and SHAM (n=2). Scale bar = 100 µm.

Microglia Increase Reactivity Within Ischemic Region To further characterize the inflammatory processes that occur after MCAO, microglial activity was assessed in a spatial manner with the immunohistology marker, Iba-1. Brain tissues from mice with induced MCAO and SHAM surgery were sacrificed and examined spatially at three days after ischemia at stereotaxic location bregma +2, +1, and 0 within the ipsilateral core, core border, and PiNT for Iba-1 expression. In the SHAM mouse cortex, Iba-1 expressing microglia exhibit a quiescent, ramified morphology (Figure 3.4)

(Nowicka 2008). After ischemia, resident microglia can increase Iba-1 reactivity, change morphology, as well as infiltrating monocytes will express Iba-1 (Ito 2001). Iba-1 expression was analyzed as mean gray value fold change and gray maxima count fold change against the contralateral side to detect regional changes in Iba-1 expression. Iba-1 regional fold changes and gray maxima count fold changes in MCAO animals were compared to SHAM animals (Figure 3.4). Iba-1 mean gray value fold change significantly decreased within the core region at bregma +2 with a fold change of 0.74 ± 0.09, a -1.3 fold change compared to SHAM (Figure 3.4d). Iba-1 gray maxima count also significantly decreased within the core region at bregma +2 with a fold change of 0.28 ± 0.2, a -3.6 fold change to SHAM (Figure 3.4e). Iba-1 gray maxima count fold change also

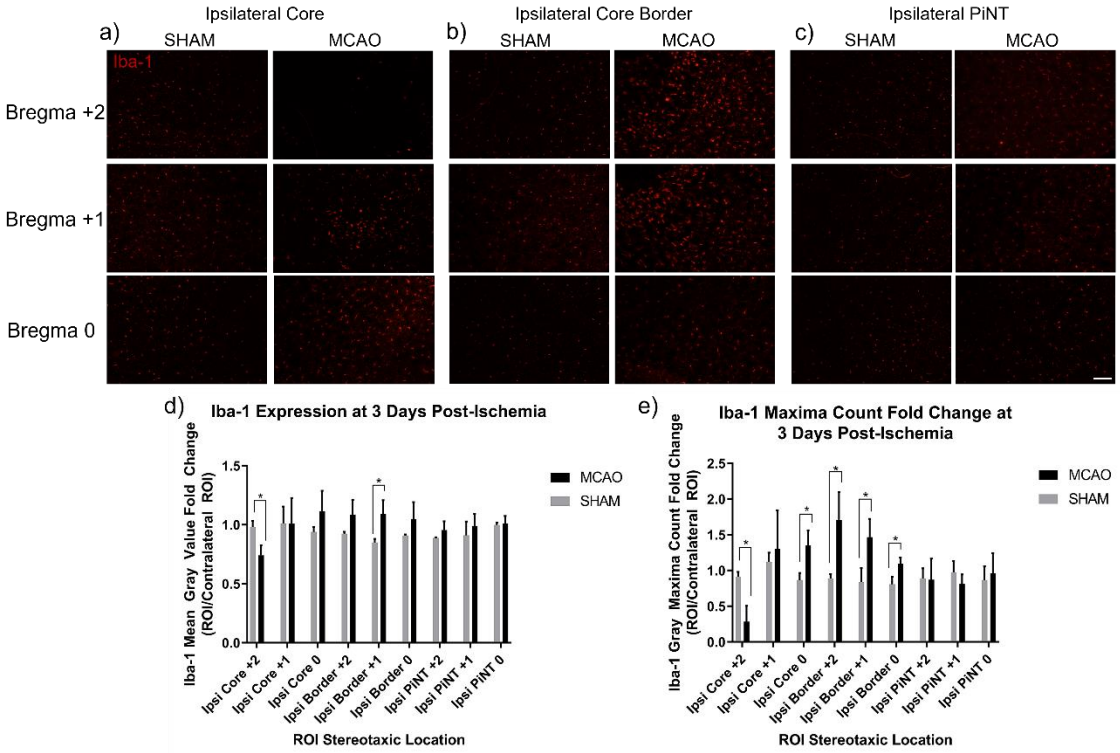

Figure 3.4 Iba-1 Expression Demonstrates Microglia Reactivity 3 Days Post-Ischemia. Brains from mice with induced MCAO were examined spatially 3 days after ischemia for Iba-1 expression. Mean gray value fold change and gray maxima count fold change of Iba-1 expression compared to the contralateral hemisphere in the ipsilateral core (a) ipsilateral core border (b) and ipsilateral PiNT (c). Mean gray value (d) fold change decreased in core region at bregma +2 and increased in the core border at bregma +1. Mean gray value fold change of Iba-1 was non-significant in PiNT or in other regions of interest at any other stereotaxic location. Gray maxima count fold change of Iba-1 decreased in ipsilateral core region at bregma +2 but increased in the core region at bregma 0 and all stereotaxic ipsilateral core border regions (e). Gray maxima count fold change of Iba-1 was non-significantly different in PiNT at all stereotaxic locations. Data are expressed as mean ± SD; $p<0.05$, MCAO (n=4) and SHAM (n=2). Scale bar = 100 µm.

exhibited a significant increase compared to SHAM within the core region at bregma 0 with a fold change of 1.35 ± 0.2. Immunohistology images (Figure 3.4a) demonstrate a distinct morphological change in Iba-1 expressing cells within the bregma +2 core region. There was also a disappearance of Iba-1 expressing cells from the center of the core region, likely reflecting within the decrease of gray values, specifically maxima count. Additionally, round Iba-1 expressing cells appear along the core border region with beginning invasion into the core, suggesting activation of residential microglia and potentially early invasion of peripheral monocytes.

Iba-1 mean gray value expression minimally increased within the core border at bregma +1 with a fold change of 1.09 ± 0.12 compared to SHAM (Figure 3.4d). Iba-1 gray maxima count fold change demonstrates significantly increased Iba-1 counts at all core border stereotaxic bregma locations (Figure 3.4e). Iba-1 gray maxima count fold change within the core border at bregma +2, bregma +1, and bregma 0 were 1.71 ± 0.4, 1.47 ± 0.2, and 1.1 ± 0.1 respectively. The increase in gray maxima count Iba-1+ round cells within each bregma core border location further suggests activation of residential microglia and early invasion of peripheral monocytes into the core in a spatial manner at three days post-ischemia. No significant changes in Iba-1 mean gray value fold changes between MCAO and SHAM were seen in ipsilateral core or core border regions at any other stereotaxic location. Additionally, Iba-1 mean gray fold change expression was non-distinct from SHAM at bregma 0. No significant changes in Iba-1 gray maxima count fold change were seen in the PiNT at any stereotaxic location. Inflammatory activation within the core border of GFAP- and Iba-1- expressing astrocytes and microglia demonstrates the importance of this region early after ischemia. Therefore, we have determined that consistent identification of the core border

can be histologically defined with combination of these three glia cell stains: FJB, GFAP, and Iba-1 at three days post-ischemia (Figure 3.5).

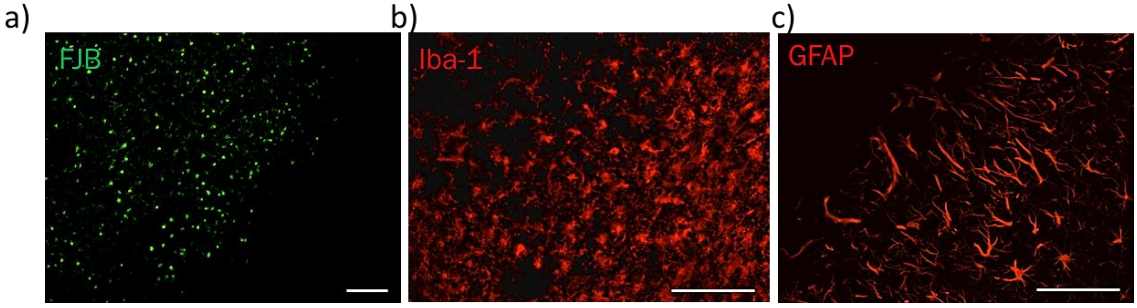

Figure 3.5 Histological Markers Define Core Border at 3 Days Post-Ischemia. Immunohistology images of FJB (a; green), Iba-1 (b; red), and GFAP (c; red) compared at the core border at bregma +2 can define a consistent, clear core border at 3 days post-ischemia. Scale bar = 100 µm.

Nanostring Digital Spatial Profiling Defines Distinct MCAO Protein Profiles In order to elucidate a detailed proteomic analysis and profile after ischemia within these specific ROI's, we utilized Nanostring's DSP technology. Brain tissues from mice with induced MCAO were sacrificed and examined spatially at three days after ischemia in the ipsilateral core border, peri-infarct, and PiNT tissues compared to the contralateral side with the Nanostring DSP Neural Cell Profiling protein panel (70 proteins; excluding IgG negative targets). Sections were immunostained with four chosen identifying markers for ROI selection (Figure 3.6). Markers included: MAP2 for neuronal damage, GFAP for astrocytic reactivity, Iba-1 for microglia, and Syto13 for nuclei. The full neural cell profiling protein panel was run on each ROI resulting in quantified protein read-outs for each ROI.

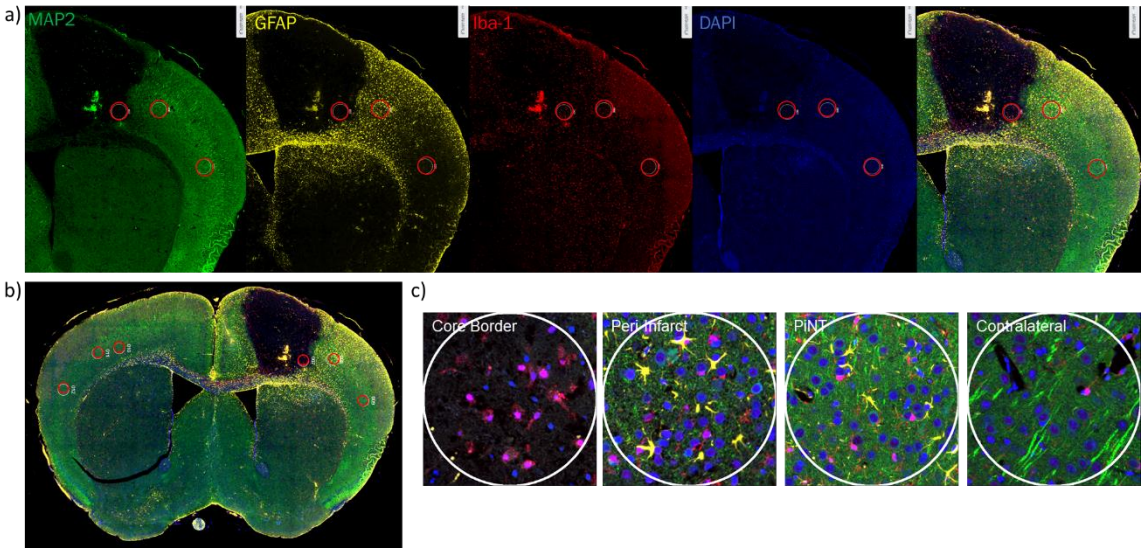

Figure 3.6 Representative Immunohistochemical Figures for DSP Analysis and ROI Selection. Coronal sections from mice with induced photothrombotic MCAO were immunohistologically stained for identifying markers MAP2 (green), GFAP (yellow), Iba-1 (red), and Syto13 for nuclei (blue) (a) and overlayed for ROI selection (b). Overlay of these markers clearly identified the extent of the infarct region and astroglia immunoreactivity within the core border. ROI's included ipsilateral core border, ipsilateral peri-infarct, ipsilateral PiNT, and contralateral cortex, each region is outlined in a red circle (c). Clear difference in the identifying IHC markers can be seen within each ROI.

To determine the comparative significance of DSP regional specific comparisons to whole tissue analysis, DSP proteomic profiles were first compared as a combined ipsilateral hemispheric group to contralateral hemispheres proteomic data. All ipsilateral ROIs (core border, peri-infarct, and PiNT ROIs) were combined as one ipsilateral hemispheric group and compared against the contralateral side for significantly changed proteins via an LMM. Then, the individual core ROI was compared against the contralateral side for significantly changed proteins via an LMM (Figure 3.7). The whole ipsilateral hemispheric group resulted in only 4 significantly upregulated proteins. However, when the ipsilateral core border ROI was isolated and compared to the contralateral tissues, 27 proteins demonstrated significant changes, with 19 upregulated and 8 downregulated.

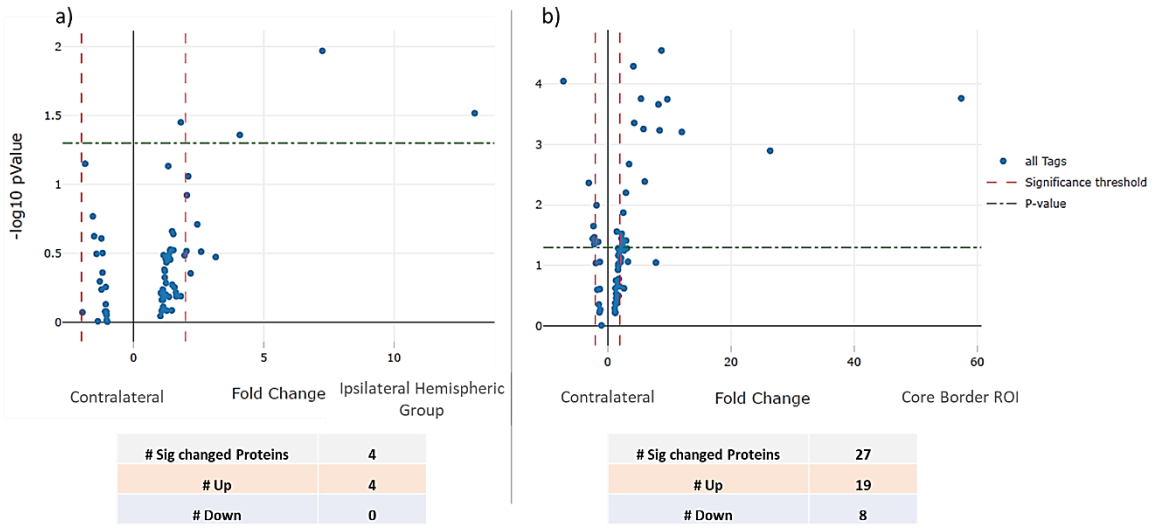

# Sig changed Proteins	4
# Up	4
# Down	0

# Sig changed Proteins	27
# Up	19
# Down	8

Figure 3.7 Ischemia Presents Region Specific Proteomic Profiles. Volcano plots representing the significant protein fold changes of the Ipsilateral Hemispheric group (core border, peri-infarct, and PiNT ROIs) (a) and isolated core border ROI (b) compared against the contralateral ROI. Data is plotted on a -log10 pValue scale; fold change on the x-axis; all tags (blue plotted dots) represent individual panel proteins; p-value (0.05; green dotted x parallel line) (n=3).

To determine general similarities and consistencies between the proteomic profiles of ROIs between biological samples, a hierarchical cluster was created (Figure 3.8). Overall, all core border ROIs clustered together, demonstrating the most similar profiles across samples within the core border. Peri-infarct ROIs clustered closest to the core border ROIs, demonstrating similarity between samples within the peri-infarct region and closest proteomic profile next to the core border ROIs. The PiNT and contralateral ROIs clustered generally together outside of the core border and peri-infarct regions, demonstrating most similarity to each other between samples and furthest similarity to the core border and peri-infarct regions. Overall, this hierarchal cluster suggests that each ROI group demonstrates a unique, consistent proteomic profile after ischemia.

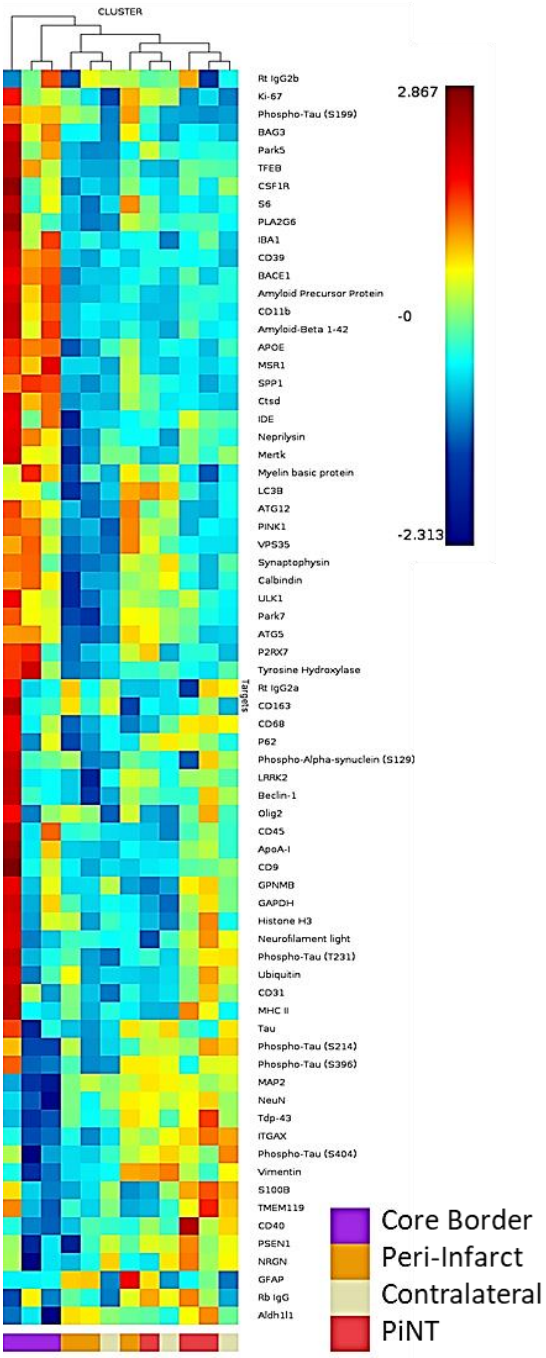

Figure 3.8 Hierarchical Cluster Heat Map of ROIs. Protein expression from each individual ROI representing the ipsilateral core border (purple), ipsilateral peri-infarct (orange), ipsilateral PiNT (red), and contralateral (white) is plotted on a heat map where red= higher representative expression and blue= lower representative expression. ROIs are clustered according to proteomic expression similarity where most similar are clustered together and tree relatives are mapped above.

Each ROI was further characterized compared to the contralateral ROI. Significantly differentially regulated proteins according to fold change were documented for each ROI (Table 2). The ipsilateral core border ROI demonstrated 27 differentially regulated proteins with 19 upregulated and 8 downregulated. Of these 27 differentially regulated proteins, there was most notably a unique profile reflected in neuronal death, apoptotic, immunoreactive, and early degeneration proteins. Neuronal proteins, MAP2 and NeuN resulted in downregulation of -7.19 and -3.07 respectively in the core border. An autophagy protein, BAG3, resulted in a 12.04-fold upregulation and a lysosomal autophagy protein, CTSD, was also upregulated by 8.44-fold. The astrocytic protein, Aldh1/1, was downregulated by -2.30-fold and a glial cytoskeletal intermediate filament protein, vimentin, was downregulated by -2.15-fold. Many proteins related to microglial immunoreactivity and immune peripheral invasion were significantly upregulated within the core border region. These included a 2.25-fold upregulation in CD45, a 4.31-fold upregulation in Iba-1, an 8.24-fold upregulation in CD11b, an 8.74-fold upregulation in CD39, and a 9.69-fold upregulation in MSR1. Notably, there was also a marked 26.39-fold upregulation in SPP1, a protein specifically associated with disease-related microglia.

Within the core border region, BACE1 was upregulated by 4.18-fold, APP was upregulated by 5.41-fold, and amyloid β (αβ) 1-42 was upregulated by 5.82-fold. This suggests that three days after ischemia, the BACE1 cleaving protein was upregulated within the core and perhaps leads to increased cleaved products of APP and the αβ 1-42 form. Notably, there was a significant upregulation of the tau-S199 amyloid by 57.42-fold, which can lead to neuronal destabilization and death. There was also a significant upregulation of ApoE by 6.02-fold, which could later lead to be neuroprotective or neurodegenerative depending on whether it is expressing the neuroprotective isoform 3 or neurodegenerative isoform 4 (Koistinaho 2005). The ipsilateral peri-infarct ROI demonstrated significant upregulation in 3 proteins: GFAP, was upregulated by 23.69-fold, tau-

S199 was upregulated by 21.41-fold, and BAG3 was upregulated by 2.96-fold. The ipsilateral PiNT ROI only demonstrated significant upregulation in one protein, GFAP, by 6.09-fold.

Table 3.2 Regulatory Proteomic ROI Profiles. Proteins were compared against the contralateral side for significant fold changes via an LMM for each ROI including: Ipsilateral Hemispheric Group, ipsilateral core border ROI, ipsilateral peri-infarct ROI, and ipsilateral PiNT ROI. Upregulated proteins expressed in yellow-green, downregulated proteins expressed in orange-red ($p<0.05$, $n=3$).

		Ipsilateral Hemispheric Group	Ipsilateral Core Border ROI	Ipsilateral Peri-Infarct ROI	Ipsilateral PiNT ROI
	Differentially Regulated Proteins	4	27	3	1
	Upregulated	4	19	3	1
	Downregulated	0	8	0	0
Protein Name	**Protein Acronym**	Fold Change	Fold Change	Fold Change	Fold Change
Microtubule associated protein 2	MAP2		-7.19		
Neuronal nuclei	NeuN		-3.07		
BAG family molecular chaperone regulator 3	BAG3	4.08	12.04	2.96	
Cathepsin D	CTSD		8.44		
Transcription factor EB	TFEB		2.96		
Vacuolar protein sorting ortholog 35	VPS35		2.36		
Aldehyde dehydrogenase 1 family member A1	Aldh1l1		-2.30		
Vimentin	VIM		-2.15		
Glial fibrillary acidic protein	GFAP	7.25		23.69	6.09
Cluster of differentiation 45	CD45		2.25		
Ionized calcium binding adaptor molecule 1	IBA1		4.31		
Cluster of differentiation molecule 11B	CD11b		8.24		
Cluster of differentiation 39	CD39		8.74		
Macrophage scavenger receptor 1	MSR1		9.69		
Secreted phosphoprotein 1	SPP1		26.39		
P2X purinoceptor 7	P2RX7	1.82	3.01		
Complement component 3 receptor 4 subunit	ITGAX		-1.53		
Beta-secretase 1	BACE1		4.18		
Amyloid Precursor Protein	APP		5.41		
Amyloid-Beta 1-42	αβ 1-42		5.82		
Phospho-Tau (S199)	tau-S199	13.10	57.42	21.41	
Phospho-Tau (S404)	tau-S404		-2.19		
Apolipoprotein E	ApoE		6.02		
Insulin-degrading enzyme	IDE		1.48		
Neprilysin	NEP		3.48		
TAR DNA-binding protein 43	Tdp-43		-1.81		
Neurogranin	NRGN		-2.42		
Parkinson Disease 5	Park5		2.54		

3.4 Discussion

Our data presented emphasizes the importance of accounting for spatial differences when analyzing post-ischemic proteomic data. Our proteomic analysis presents unique profiles spatially and regionally in relation to the infarct core. Previous technologies using whole ipsilateral tissues can provide some insight into mechanisms occurring post-ischemia but can greatly obscure specific mechanisms that occur within each region. Our data demonstrated that each region analyzed with

DSP demonstrated a unique proteomic profile with distinctly regulated proteins. Within the ischemic core border, a unique profile relating to neuronal death, apoptosis, immunoreactivity, and early degeneration was identified. When looking further into the relationship between these differentially regulated proteins, a potential pattern emerged with future interest for therapeutic targeting. As expected, the neuronal proteins, MAP2 and NeuN were downregulated, indicative of neuronal death within the core border. This is also reflected in the upregulation of the autophagic protein, BAG3, and the lysosomal autophagy protein, CTSD. CTSD has been shown to increase sharply after ischemia but will decrease as lysosomes rupture (Liu 2019). BAG3 was also upregulated within the peri-infarct region, suggesting that autophagy and related apoptosis may still be ongoing within this region.

Ischemia also resulted in an upregulation of the general immune cell surface marker, CD45, as well as Iba-1. This suggests an increase in residential microglia and/or peripheral monocyte infiltration and activity. However, as residential microglia are recognized to decrease acutely within the core via degeneration, which is reflected within the immunohistochemistry mean gray value and gray maxima count fold changes, we expect this Iba-1 increase to reflect peripheral monocyte invasion (Ito 2001; Matsumoto 2007; Nowicka 2008). This is also suggested by the 8-fold upregulation of CD11b and CD39 and a 3-fold upregulation of the CD39 receptor, P2RX7, which are all surface markers on leukocytes. Leukocytes are noted to begin infiltrating into the ischemic region as early as 12 hours after ischemia and persist, with peak levels at 7 days post-ischemia (Nowicka 2008; Ito 2001; Sanchez-Bezanilla 2021). Microglia reactivity post-ischemia is notoriously recognized to have both beneficial and deleterious effects. Activated microglia acutely can phagocytose cells that have necrotized within the lesion core, preventing the further release of neurotoxic products (Giulian 1993a, 1993b; Matsumoto 2007). However, activated microglia also release many pro-inflammatory cytokines and reactive oxygen species which can contribute to

infarct development (Giulian 1993a, 1993b; Matsumoto 2007). Therefore, truly understanding the interactions of these cytokines and proteins is key to identifying future targets for therapeutic intervention. For example, CD39 and MSR1 both demonstrated an upregulation of approximately 9-fold, and both proteins have been suggested to play a neuroprotective role within the inflammatory process. Transgenic mouse lines overexpressing CD39 resulted in reduced leukocyte infiltration, smaller infarct volumes, and decreased neurological deficit after ischemia, suggesting a neuroprotective role of CD39 during ischemic insult (Baek 2017). CD39 expression on endothelial cells and leukocytes is suggested to reduce inflammatory cell trafficking and platelet reactivity via cell-cell interaction after ischemia (Hyman 2009). Also, it has been shown that higher expression of the MSR1 protein increases damaged-associated molecular patterns (DAMP) clearance after ischemia via MSR1-induced resolution of neuroinflammation, indicating MSR1 as a potential therapeutic target (Zou 2021). Additionally, there was a notable, 57-fold upregulation of the protein SPP1. This protein is suggested to function as a pro-angiogenic trophic factor, but it is also associated with neurodegeneration as it is recorded to be upregulated in senescent microglia in an age-dependent manner (Li 2010; Jiang 2020). Controversially, this protein has also been associated with macrophagic communication to astrocytic migration toward the infarct area that has been suggested to be a neuroprotective repair mechanism of the ischemic neurovascular unit early after ischemia (Choi 2019).

A unique astrocytic proteomic profile is reflective throughout each region. Within the core border, there is downregulation of the astrocytic proteins, Aldh1/1 and vimentin by about 2-fold. Vimentin-expressing astrocytes have been shown to increase acutely after ischemia but given downregulation at this three-day timepoint in combination with Aldh1/1 downregulation, may suggest astrocytic degeneration within the core (Kindy 1992). However, large upregulation of GFAP within the peri-infarct region by almost 24-fold and confirmed with mean gray value fold

change increase at the core border both in stereotaxic location bregma +2 and +1 suggests strong reactivity of astrocytes within the border and peri-infarct region three-days after ischemia. GFAP has been shown by multiple studies to be increased specifically within the peri-infarct region beginning as early as 4 hours after ischemia up until 28 days (Kindy 1992; Nowicka 2008; Sanchez-Bezanilla 2021). Reactivity of astrocytes and microglia can lead to secondary tissue damage, progressive cavitation, and scar formation along the peri-infarct border (Fitch 1999). Ultimately, the relative differences between these microglial and astrocytic proteomic profiles within the core border and peri-infarct regions could provide potential targets for prevention of secondary damage and anti-inflammation.

Ischemia is well-recognized to be associated with neurodegeneration and more specifically the relationship between stroke history, tau proteins, and increased Alzheimer's Disease prevalence (Sun 2006; Zheng 2010). Multiple tau related proteins within the core border region resulted in a pattern that could ultimately indicate a future therapeutic target. BACE1, APP, and αβ 1-42 all demonstrated an approximate 5-fold upregulation within the core border. BACE1 has been shown to be upregulated in response to released reactive oxygen species and hypoxia inducible factor 1α (HIF1α) following ischemia (Sun 2006; Guglielmotto 2009). Increased BACE1 activity results in increased cleavage of APP with increased deposits and aggregation of the neurotoxic form of amyloid β, αβ 1-42 (Sun 2006; Guglielmotto 2009). BACE1 expression was found to be regulated by a positive feedback loop between γ- and β-secretase cleavages on APP (Wang 2006; Li 2009). Additionally, upregulation of APP within neurons, astrocytes, or microglia can lead to neuronal destabilization and vulnerability to stress, suggesting that upregulation of all three proteins within the core border could be indicative of a neurodegenerative profile (Koistinaho 2005). The tau-S199 form was also found highly upregulated by 57-fold within the core border, and this tau form has been shown to play a role in the development of Alzheimer-like lesions after ischemia. After

ischemia, tau proteins become rapidly dephosphorylated acutely and are then slowly rephosphorylated and accumulated in a serine site-specific manner (Zheng 2010). Tau-S199 has been reported to be specifically induced after ischemia and to contribute to ischemic neuronal injury (Zheng 2010). Dysregulation and displacement of tau proteins after ischemia is suggested to contribute to a neurodegenerative profile. Lastly, upregulation of the protein ApoE within the core border region could play a dual role depending on the isoform of ApoE that is being expressed. ApoEε3 is the most common isoform and can exhibit a neuroprotective effect by contributing to communication from microglia to neurons for repair, regeneration and survival as well as suppression of microglia reactivity (Koistinaho 2005). However, the ApoEε4 isoform may be neurodegenerative by contributing to αβ deposition (Koistinaho 2005).

Chapter 4: Delayed Neuregulin-1 Treatment Induces a Late Neuroprotective and Early Regenerative Proteomic Profile

4.1 Introduction

Our lab and others have previously demonstrated that exogenous NRG-1 treatment significantly decreases acute neuronal death and neuroinflammation after ischemic damage with a therapeutic window of >12 hours (Shyu 2004; Xu 2004, 2006; Li 2007b, 2008; Guan 2015; Noll 2019). NRG-1 has also demonstrated a direct neuroregenerative effect with increased neuronal sprouting, synapse formation markers, and functional recovery 3 weeks after ischemia (Iaci 2010, 2016). However, the spatial neuroprotective and early regenerative effects of NRG-1 following ischemia have not been clearly elucidated. In this study, we examined how delayed NRG-1 treatment alters the spatial MCAO proteomic profiles as defined in Chapter 3 and can continue to act as a prolonged ischemic stroke therapeutic. By utilizing the photothrombotic MCAO model and

Nanostring Digital Spatial Profiling (DSP) to analyze NRG-1 treated coronal brain sections at 3-days post-ischemia in comparison with immunohistochemical data, we have more specifically identified the proteomic profile of NRG-1 treatment after ischemia in a spatial manner. Our data suggests that delayed NRG-1 treatment induces a unique spatial proteomic profile 3-days post ischemia by inducing autophagy and mitophagy in neurons and microglia, immune cell phagocytosis, and synaptic activity to enhance neuroprotection via resistance to apoptosis and priming of a neuroregenerative niche.

4.2 Materials and Methods

Animals All animals used in these studies were treated humanely and with regard for alleviation of suffering and pain, and all protocols involving animals were approved by the IACUC of University of California-Riverside prior to the initiation of experimentation. Male and female C57BL6 mice (8–10 weeks old) were purchased from Jackson Laboratories (Bar Harbor, Maine) and housed with a 12-hour daily light/dark cycle. Food and water were provided ad libitum. All surgical procedures were performed by sterile/aseptic techniques in accordance with institutional guidelines.

Photothrombotic Middle Cerebral Occlusion Animals were subjected to left photothrombotic MCA occlusion (MCAO). Mice were anesthetized with 2% isoflurane and circulating air (N2O:O2 at approximately 2:1) and maintained anesthetized during the procedure via a modified gas tubing nose connection on a stereotaxic instrument. Eye lubricant was applied to protect the eyes and body temperature was maintained via a heating pad placed underneath the mice during surgery at 37°C. MCAO was performed in an adapted accordance to Zhong et al. (Zhong 2010). Rose Bengal (10 mg/mL; Cat#330000, Sigma, Burlington, MA) was injected intraperitoneally (i.p.) at 10 mL/g and

allowed to incubate for 8 minutes. The animal was stabilized in the stereotaxic instrument and the scalp hair was removed. The scalp was disinfected with iodine and ethanol, then followed by a midline skin incision to expose the skull above the left sensorimotor cortex. A 2-mm diameter focal green laser (520nm; Cat# LP520-MF100 ThorLabs Inc, Newton, NJ) was directed at 2-mm lateral left and 0.6-mm posterior of bregma. Laser irradiation occurred for 20 minutes at 10 mW. After irradiation, the midline incision was sealed with Vetbond glue followed by triple antibiotic. Mice were then placed into a 37°C incubation chamber for 20-30 minutes to recover.

To determine how NRG-1 treatment may alter the spatial proteomic MCAO profiles as defined in Chapter 3, mice were divided into two treatment groups and injected i.p. with either a daily 100-μL dose of vehicle (0.1% BSA in PBS) or NRG-1β (5ug/kg/day NRG-1 (EGF-like domain, R&D Systems, Minneapolis, MN) in 1% BSA in PBS) beginning 24 hours after surgery and sacrificed at 3 post-ischemia (dpi). Mice designated for immunohistochemistry analysis were randomized and blinded where 3dpi NRG-1 (n= 3) and vehicle (n= 4). Mice designated for Nanostring DSP analysis were unblinded where 3dpi NRG-1 (n = 3) and compared to previous DSP MCAO analysis data from Chapter 3.

Histology and Immunohistochemistry After MCAO, mice were deeply anesthetized with 2% isoflurane and perfused transcardially with saline followed by cold 4% paraformaldehyde (PFA) solution. Brains were quickly removed and maintained in 4% PFA for 24 hours. Brains in preparation for histological and immunohistochemical analysis were quickly removed after transcardial perfusion and maintained in 4% PFA for 24 hours before being cryoprotected in 30% sucrose. The brains were then flash frozen and stored at – 80°C until sectioning. Coronal sections of 12–15 μm thickness were cryosectioned and mounted on slides which were then stored at −80°C until further processed.

Fluoro Jade B (FJB; Cat#AG310, Millipore, Billerica, MA) labeling was performed in an adapted accordance to Noll 2019 to ensure infarct presence and record infarct size and location (Noll 2019). Sections were post-fixed with 10% formalin for 10 minutes and then washed twice with PBS for 5 minutes. Sections were then directly incubated in 0.06% potassium permanganate (KMnO4) for 3 minutes followed by distilled water for 2 minutes. Sections were then incubated in a freshly prepared solution of 0.0004% FJB with DAPI for 20 minutes, rinsed in distilled water 3 times for 2 minutes, and then dried at 50°C.

For immunohistochemical studies, sections were dried at room temperature for 30 minutes. After rinsing with 0.01M PBS, sections were blocked in PBS containing 5% normal donkey serum and 0.1% Triton X-100 for 1-2 hours at room temperature, rinsed with PBS/0.2% Tween-20 (PBST) and then incubated overnight at 4°C with primary antibodies of polyclonal rabbit anti-Iba-1 (1:1000, Cat#019-19741, Wako, Osaka, Japan) and Cy3-conjugated monoclonal mouse anti-GFAP (1:400, Cat#C9205, Sigma, Burlington, MA). Sections were washed 3 times with PBST, incubated with respective AlexaFluor594-conjugated donkey anti-rabbit IgG antibody (1:400, Cat#711-585-152, Jackson ImmunoResearch Laboratory, West Grove, PA) for 1 hour at room temperature, then rinsed 4 times with PBST before mounting with DAPI-Fluoromount-G (Cat#OB010020, Fisher Scientific, Pittsburgh, PA).

Immunohistochemical Quantification A Leica DM5500 B Automated Upright fluorescence microscope was used to capture all digital images of FJB stained sections at x5 magnification. A Nikon TS2-S-SM inverted fluorescence microscope equipped with a CCD camera was used to capture all digital images of sections at ×10 magnification.

Immunohistology images of FJB+ cells were captured at bregma +2 and +1 at 5x magnification to capture the entire image area of FJB+ cells. Images were taken at the ipsilateral

core and corresponding contralateral cortical region of three separate tissue sections for each mouse. FJB+ cells were counted semi-automatically with ImageJ software (Media Cybernetics, Inc., Bethesda, MD) after threshold at size 10-infinity (pixel units) and circularity 0.4-1.00. FJB+ cell counts were averaged for each stereotaxic location. FJB+ cell counts were compared between NRG-1 and vehicle treatment groups with student two sample t-tests assuming unequal variances.

Immunohistology images of Iba-1, and GFAP were captured at approximately bregma +2, +1, and 0 at four different regions of interest: the core, core border, PiNT and contralateral cortex in three separate corresponding tissue sections for each mouse according to Figure 3.1. Mean gray values were calculated with ImageJ software. All picture properties were obtained and ensured for consistency. Pictures were converted to 32-bit gray before analysis, and pictures were not altered in any other way. Area fraction was utilized as a control where all picture values must have 100% area fraction. Mean gray value regions of interest technical replicates were averaged and were calculated as fold changes against the contralateral side. Iba-1 maxima count was analyzed with prominence=15, in areas of high tissue damage where background signal may be higher, prominence was increased to 18. Maxima count ROI technical replicates were averaged and calculated as fold changes against the contralateral side. NRG-1 and vehicle treatment group fold-changes were compared using student two sample t-tests assuming unequal variances to determine statistically significant treatment effects.

Formalin-Fixed Paraffin Embedded Tissue Preparation Brains in preparation for Nanostring DSP were continually dehydrated in preparation for paraffin embedding: 24 hours of 4% PFA was followed by 24 hours each in 40% ethanol, 70% ethanol, and a second change of 70% ethanol. Brains were then placed whole into cassettes and processed in a Tissue-Tek Processor in a 12-hour cycle (Table 3.1) before embedding coronally in paraffin.

Table 3.1. Tissue-Tek Processing Protocol

Reagent	**Time**
Ethanol	30 minutes
Ethanol	5 x 1 hour
CitriSolv	3 x 45 minutes
Wax	3 x 1 hour

Formalin-fixed, paraffin-embedded (FFPE) samples were sectioned to approximately bregma +2 and 5-μm thickness sections were mounted onto slides and allowed to dry at room temperature overnight. FJB labeling was performed as described above to ensure infarct presence and record infarct size and location. Samples confirmed with FJB+ cells indicating successful MCAO were sent to Nanostring (Seattle, WA) for slide mounting and GeoMx DSP profiling.

Nanostring Digital Spatial Profiling Analysis To visualize whole tissue, mounted slides were stained with oligo-conjugated antibodies for MAP2, Iba-1 and GFAP, and with Syto13 (nuclei) in the GeoMx DSP instrument. Circular geometric patterns (200 μm diameter) were used to identify six ROIs on the scanned tissues of each sample: core border, peri-infarct, and PiNT regions on ipsilateral and contralateral hemispheres. The GeoMx Neural Cell Profiling protein panel (73 proteins) was utilized for this analysis. UV-cleavable oligo-conjugated antibodies according to the panel were dispensed onto each ROI, UV-cleaved off, aspirated into a plate, hybridized and counted by the GeoMx DSP instrument. All resulting spatial, quantified analysis was performed in the Nanostring GeoMx DSP analysis software. Background correction was determined by protein target correlation plot and high correlation was seen between Rb IgG and Rb IgGa proteins and were used for panel background correction via signal-to-background ratio. Spatial ROIs were compared using a linear mixed model (LMM) with BH correction and random effect for Scan ID and ROI ID. Fold changes were identified by comparing individual ROIs against the contralateral ROI with a significance of $p\ value<0.05$.

4.3 Results

FluoroJadeB Demonstrates No Difference with NRG-1 Treatment at 3 Days Post-Ischemia

We examined the infarct and possible prevention of neurodegeneration at three days in vehicle and NRG-1 treated mice post-injury with the chemical neurodegenerative stain, FJB. Brain tissues from mice with induced MCAO and blindly treated with vehicle or NRG-1 were sacrificed and examined spatially at three days after ischemia at bregma +2 and +1. FJB+ cells were found throughout the infarct core at bregma +2 with no difference in cell number between treatment groups (Figure 4.1). Vehicle group exhibited a mean of 547.3 ± 114 and NRG-1 treatment exhibited a mean of 461.4 ± 156 at bregma +2. FJB+ cells were not significantly found at bregma +1 in either treatment group. Vehicle group exhibited a mean of 11.6 ± 19 and NRG-1 treatment exhibited a mean of 1.3 ± 0.7 at bregma +1. This demonstrated that NRG-1 treatment appears not to have a direct effect on neurodegenerative damage detectable by FJB staining three days after MCAO at bregma +2.

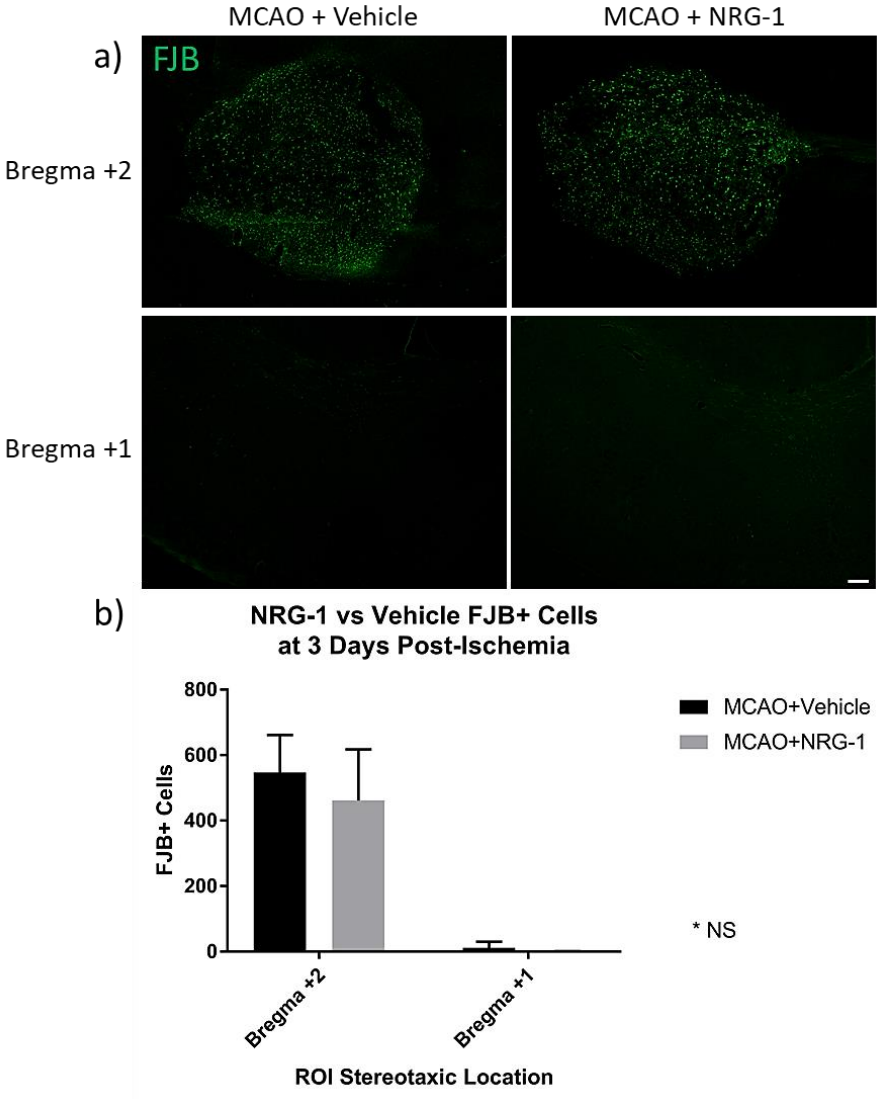

Figure 4.1 FJB Demonstrates No Difference with NRG-1 Treatment at 3 Days Post-Ischemia. Brains from mice with induced MCAO and blindly treated with vehicle or NRG-1 were examined 3 days after MCAO. a) Representative FJB images of MCAO+Vehicle and MCAO+NRG-1 treatment groups at bregma +2 and +1 at x5 magnification. FJB+ cells were counted at bregma +2 and +1 at x5 magnification for whole infarct comparison. b) FJB+ cells were found throughout the infarct core at bregma +2 with no difference in cell number between treatment groups. FJB+ cells were not significantly found at bregma +1 in either treatment group. A mean value of FJB+ cells from three brain sections from each location was obtained for each individual mouse brain (c; $p<0.01$, MCAO+Vehicle (n=4) and MCAO+NRG-1 (n=3)). Data are expressed as mean ± SD. Scale bar = 100 µm.

GFAP and Iba-1 Demonstrate No Difference with NRG-1 Treatment at 3 Days Post-Ischemia

To further characterize how NRG-1 treatment may affect the early inflammatory processes that occur after MCAO, astrocytic and microglial activity was assessed in a spatial manner with the immunohistology markers, GFAP and Iba-1, respectively. Brain tissues from mice with induced MCAO and blindly treated with vehicle or NRG-1 were sacrificed and examined spatially at three days after ischemia at bregma +2, +1, and 0 within the ipsilateral core, core border, and PiNT for GFAP and Iba-1 expression.

GFAP expression was analyzed as mean gray value fold change against the contralateral side to detect regional changes in GFAP expression. GFAP regional fold change expression in MCAO animals was compared between treatment groups (Figure 4.2). No significant changes in GFAP mean gray value fold changes between MCAO+Vehicle and MCAO+NRG-1 treatment groups were seen in any regions at any stereotaxic location.

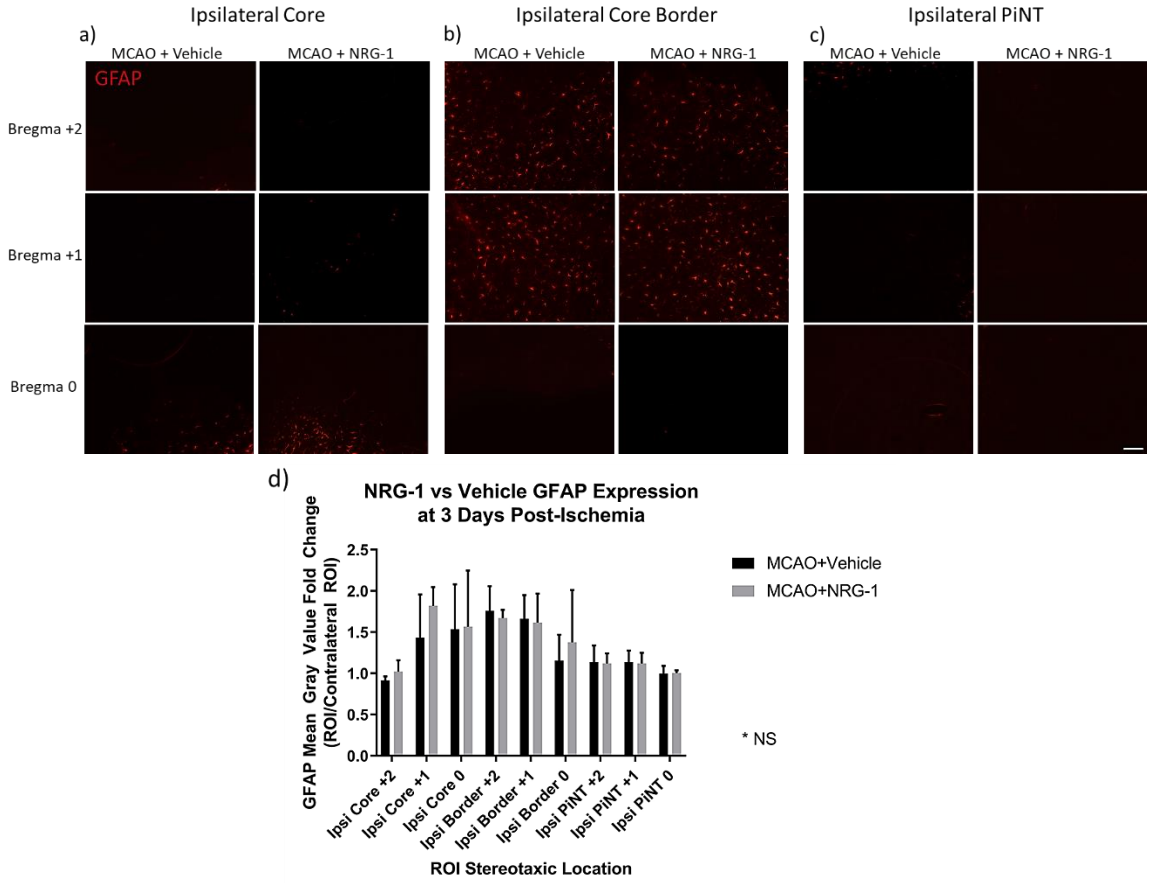

Figure 4.2 GFAP Demonstrates No Difference with NRG-1 Treatment at 3 Days Post-Ischemia. Brains from mice with induced MCAO and blindly treated with vehicle or NRG-1 were examined spatially 3 days after MCAO for GFAP expression. Mean gray value fold change of GFAP expression in MCAO+Vehicle and MCAO+NRG-1 treated groups compared to their respective contralateral hemisphere in the (a) ipsilateral core, (b) ipsilateral core border, and (c) ipsilateral PiNT. (d) Mean gray value fold change was non-significant changes between MCAO+Vehicle and MCAO+NRG-1 treatment groups in all regions at all stereotaxic locations. Data are expressed as mean ± SD; $p<0.05$, MCAO+Vehicle (n=4) and MCAO+NRG-1 (n=3). Scale bar = 100 µm.

Iba-1 expression was analyzed as mean gray value fold change and gray maxima count fold change against the contralateral side to detect regional changes in Iba-1 expression. Iba-1 regional fold changes and gray maxima count fold changes in MCAO animals was compared between treatment groups (Figure 4.3). No significant changes in Iba-1 mean gray value fold changes or gray maxima count fold changes between MCAO+Vehicle and MCAO+NRG-1 treatment groups were seen in any regions at any stereotaxic location. This suggests that if delayed

NRG-1 treatment has a spatial immunomodulatory effect, it is not reflected in GFAP or Iba-1 immunohistology expression at three days post-ischemia.

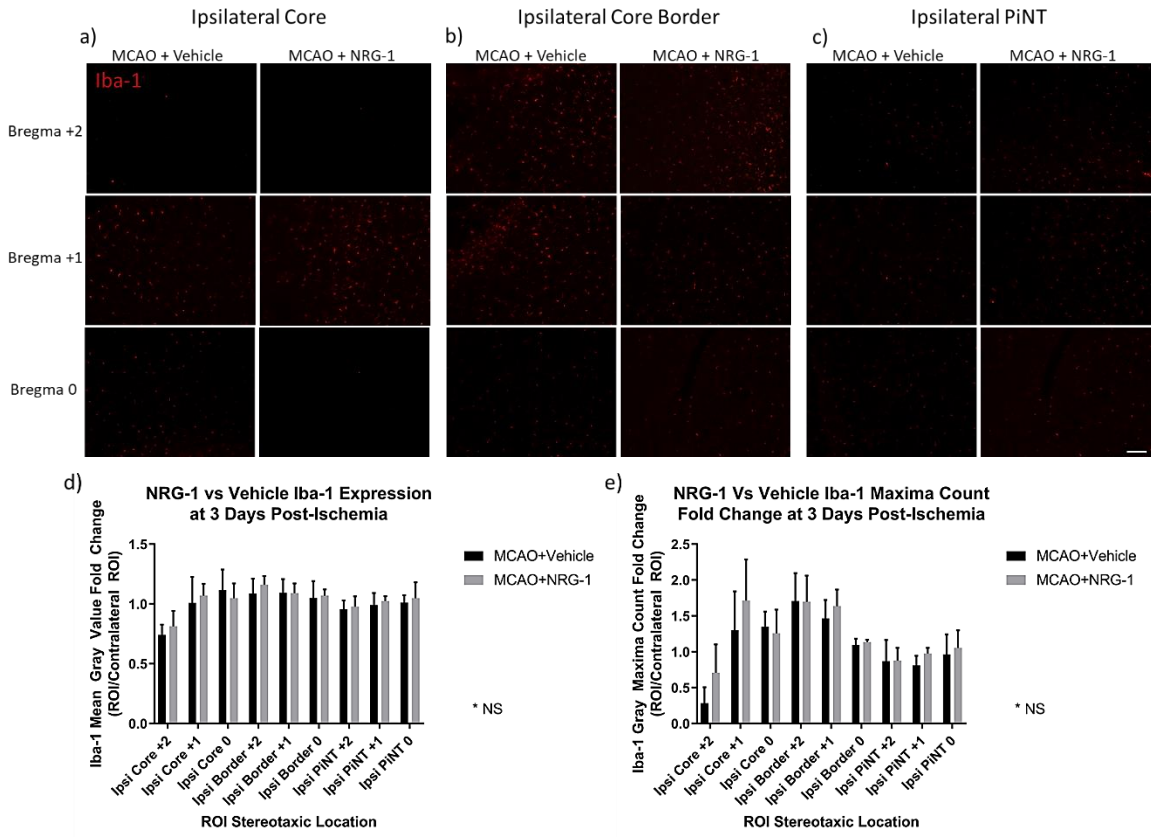

Figure 4.3 Iba-1 Demonstrates No Difference with NRG-1 Treatment at 3 Days Post-Ischemia. Brains from mice with induced MCAO and blindly treated with vehicle or NRG-1 were examined spatially 3 days after MCAO for Iba-1 expression. Mean gray value fold change and gray maxima count fold change of Iba-1 expression in MCAO+Vehicle and MCAO+NRG-1 treated groups compared to their respective contralateral hemisphere in the (a) ipsilateral core, (b) ipsilateral core border, and (c) ipsilateral PiNT. (d) Mean gray value fold change was non-significant changes between MCAO+Vehicle and MCAO+NRG-1 treatment groups in all regions at all stereotaxic locations. (e) Gray maxima count fold change of Iba-1 was non-significant changes between MCAO+Vehicle and MCAO+NRG-1 treatment groups in all regions at all stereotaxic locations. Data are expressed as mean ± SD; $p<0.05$, MCAO+Vehicle (n=4) and MCAO+NRG-1 (n=3). Scale bar = 100 µm.

Delayed NRG-1 Treatment Elucidates a Late Neuroprotective and Early Regenerative Profile with Nanostring Digital Spatial Profiling Our data suggests that with delayed NRG-1 treatment, characterizing a potential therapeutic spatial proteomic profile after ischemia extends beyond gross cellular structure found with general immunohistochemical methods. To further elucidate if NRG-

1 treatment initiates a delayed spatial therapeutic effect, we utilized Nanostring's Digital Spatial Profiling (DSP) technology and compared results to the previously defined MCAO 3dpi proteomic spatial profile.

Brain tissue from mice with induced MCAO and treated with NRG-1 were examined spatially three days after ischemia in the ipsilateral core border, peri-infarct, and PiNT in contrast to the respective contralateral side with the Nanostring DSP Neural Cell Profiling protein panel (70 proteins; excluding IgG negative targets). Sections were immunostained with four chosen identifying markers for region of interest selection (Figure 4.4). Markers included: MAP2 for neuronal damage, GFAP for astrocytic activity, Iba-1 for microglia reactivity, and Syto13 for nuclei. ROIs include the ipsilateral core border, ipsilateral peri-infarct, ipsilateral PiNT, and contralateral cortex corresponding to the core border. The full neural cell profiling protein panel was run on each ROI resulting in quantified protein read-outs for each ROI.

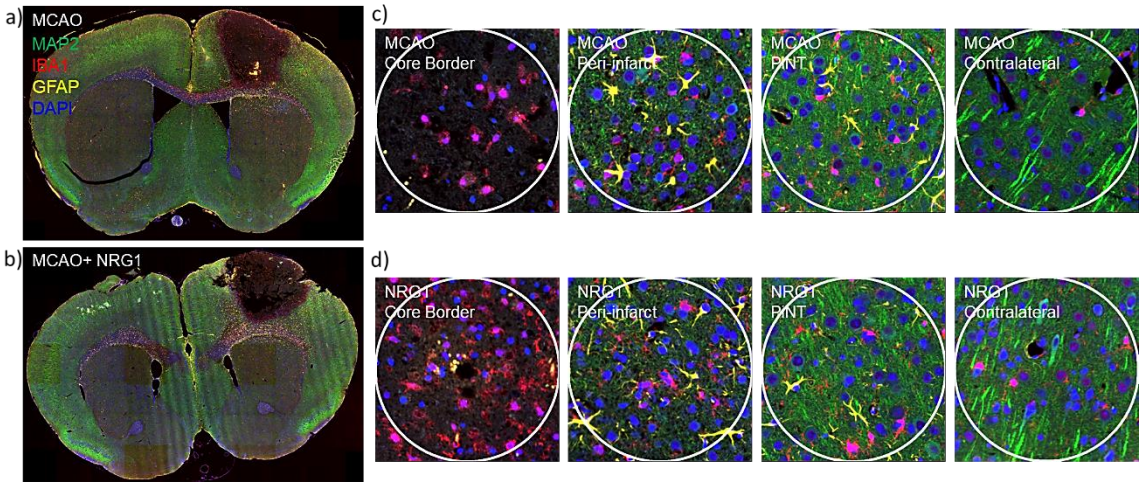

Figure 4.4 Representative Immunohistochemical Figures for DSP Analysis and ROI Selection. Coronal sections from mice with (a) induced MCAO and treated with (b) NRG-1 were immunohistochemically stained for identifying markers MAP2 (green), GFAP (yellow), Iba-1 (red), and Syto13 (blue) and overlayed for ROI selection. Higher magnification images demonstrating the selected ROIs for (c) MCAO and (d) NRG-1 treated groups. ROIs between MCAO and MCAO+NRG-1 treated groups appear similar between each corresponding region.

To further elucidate if delayed NRG-1 treatment initiates a prolonged neuroprotective spatial proteomic therapeutic effect, each ROI was further characterized compared to the contralateral ROI and compared to the previously defined MCAO proteomic spatial profiles in Chapter 3 Table 3.2. Significantly differentially regulated proteins for NRG-1 treated samples are documented for each ROI in Table 4.2 comparative to fold changes found from Chapter 3 Table 3.2 fold change values (Table 4.2). The ipsilateral core border ROI demonstrated the most altered proteomic profile indicative of a late neuroprotective and early regenerative profile with NRG-1 treatment. NRG-1 treatment in the core border region demonstrated 37 total differentially regulated proteins, 33 upregulated and 4 downregulated, compared to the MCAO profile that demonstrated 27 total differentially regulated proteins, 19 upregulated and 8 downregulated. These 37 differentially regulated proteins with NRG-1 treatment within the core border region suggest a late neuroprotective and early regenerative profile reflected in increased autophagy and mitophagy, immune cell phagocytosis, and synaptic activity indicative of neuroprotection against further neuronal apoptosis and priming of a neuroregenerative niche.

Neuronal proteins, MAP2 and NeuN resulted in essentially the same downregulated fold changes in both treatment groups. MAP2 in MCAO resulted in a -7.19-fold downregulation and NRG-1 treatment resulted in -6.88-fold change. NeuN had a downregulation of -3.07-fold with MCAO and NRG-1 treatment with a -2.20-fold change. However, delayed NRG-1 treatment induced a significant upregulation in the expression of the synaptic outgrowth factor, synaptophysin, with a 2.10-fold change increase. As also demonstrated with FJB staining, this indicates that delayed NRG-1 treatment does not significantly alter overall neuronal death, but it has an early stimulating effect on the neuroregenerative outgrowth environment.

The intermediate filament, vimentin was significantly downregulated in MCAO by -2.15-fold but demonstrated no significant differentiation with NRG-1 treatment. The astrocytic marker,

Aldh1/1 was also downregulated by -2.15-fold in MCAO but demonstrated no significant differentiation with NRG-1 treatment. This suggests that NRG-1 treatment may maintain astrocytic activity within the core border region after ischemic stroke, and as vimentin can be secreted by astrocytes to induce an axonal growth environment, this may contribute to a neuroregenerative post-stroke environment (Shigyo and Tohda 2016). There was no GFAP seen within the core border, but it was similarly upregulated in MCAO and NRG-1 treatment groups in both the peri-infarct and PiNT, as also demonstrated with IHC mean gray fold changes. MCAO demonstrated a 23.69-fold upregulation of GFAP within the peri-infarct, and NRG-1 treatment demonstrated a 29.97-fold increase. MCAO demonstrated a 6.09-fold upregulation of GFAP within the PiNT, and NRG-1 treatment demonstrated a 5.36-fold increase. However, NRG-1 treatment did have a significant increase of Aldh1/1 of 2.32-fold within the peri-infarct and a 1.59-fold in the PiNT. NRG-1 treatment also induced upregulation of the proliferation protein, Ki-67, within the peri-infarct region by 2.48-fold. This suggests that although GFAP activity of astrocytes may not differ between treatment groups, there may be a difference in astrocytic proliferation or viability within these regions.

Elucidating the importance and effects of autophagy processes in ischemic stroke remain complex and controversial. However, autophagy remains a critical process for maintaining cellular homeostasis via intracellular degradation (Klionsky 2016). In the context of stroke, understanding the cellular types that are undergoing autophagy, what types of autophagy, and whether the autophagy processes are in flux (successful degradation) or blocked is key for characterizing a neuroprotective component from a neurotoxic one (Kotoda 2018). We show for the first time that delayed NRG-1 treatment may induce late neuroprotection through the induction of autophagy and microautophagy after ischemic stroke. MCAO and NRG-1 treatment profiles show no difference between autophagy proteins, BAG3, TFEB, and CTSD within the core border region, which could

be indicative of autophagic blockage. With BAG3 activity upregulated to 12.04-fold in MCAO and 12.71-fold with NRG-1 treatment, TFEB activity upregulated to 2.96-fold in MCAO and 3.27-fold with NRG-1 treatment, and CTSD activity upregulated to 8.44-fold in MCAO and 9.97-fold with NRG-1 treatment. BAG3 was also upregulated within the peri-infarct region by NRG-1 treatment with 2.96-fold increase at MCAO and 4.52-fold increase with NRG-1 treatment. However, NRG-1 treatment also induces the upregulation of ULK1, LC3B, ATG5, PINK1, and Park7 within the core border region, suggesting successful autophagic flux restoration. ULK1 indicates the induction of autophagy, with a 1.99-fold increase. LC3B in conjunction with ATG5 indicates phagophore expansion, autophagosome formation, and elevated autophagy flux (Klionsky 2016). NRG-1 treatment increased ULK1 by 1.99-fold, LC3B by 1.58-fold, and ATG5 by 2.15-fold. Stabilized PINK1 indicates that mitochondrial damage has occurred, damaged mitochondria is accumulating, and that successful mitophagy of damaged mitochondria is occurring (Klionsky 2016). NRG-1 treatment demonstrated an increased PINK1 expression of 2.73-fold. Lastly, Park7 has been indicative of antioxidant and neuroprotective responses after ischemia in neuronal cells (Yanagida 2009). NRG-1 treatment increased Park7 expression by 1.95-fold within the core border region. Taken together, this suggests that NRG-1 treatment compared to MCAO restores autophagic and mitophagic flux after ischemia allowing for restoration for proper removal of degraded, misfolded, and damaged proteins and mitochondria in an antioxidant and neuroprotective manner.

Proteins related to microglial immunoreactivity and immune peripheral invasion were also investigated with delayed NRG-1 treatment within the proteomic panel. Iba-1, as also demonstrated by immunohistochemistry, did not show any difference between groups, and was upregulated approximately 4-fold in both groups with no significant difference in the peri-infarct or PiNT regions. There was also no clear difference seen in CD11b or CD45 in the core border region. With CD11b activity upregulated to 8.24-fold in MCAO and 9.02-fold with NRG-1 treatment, and CD45

activity upregulated to 2.25-fold in MCAO and 2.40-fold with NRG-1 treatment. NRG-1 treatment demonstrated an increase in Mertk, a phagocytic expressing protein of myeloid cells, within the core border with a 2.68-fold increase. NRG-1 also decreased CD39 activity in the core border with 8.74-fold increase in MCAO and a 5.26-fold increase with NRG-1 treatment. CD39 is highly expressed by Tregs but is also expressed on other peripheral invading cells such as neutrophils, monocytes, and lymphocytes (Antonioli 2013). MSR activity was slightly decreased by NRG-1 treatment within the core border region, with 9.69-fold increase at MCAO and 8.15-fold increase with NRG-1 treatment but was increased in the peri-infarct region with 1.85-fold upregulation. MSR1 is a macrophage receptor that assists in clearance of DAMPs, and high expressing MSR1 cells express less inflammatory cytokines and are sources for the neurotrophic factor, IGF-1 (Zhu 2019). NRG-1 treatment also demonstrated an upregulation in CD9, CSF1R, and MHC II within the core border region. NRG-1 treatment increased CD9 expression by 2.58-fold. CD9 expression is associated with exosome release from microglia and can play a complex role in inflammation (Gao 2020; Huang 2018; Zagrean 2018). CSF1R expression was increased by 2.13-fold. CSF1 receptor upregulation on microglia and neurons after ischemia can be stimulated by CSF1 release by astrocytes to promote survival and microglial response to injury (Wang 1999). MHCII, an antigen presenting surface marker on M1-like microglia and macrophages, was upregulated by 1.49-fold. NRG-1 treatment also upregulated the expression of Myelin Basic Protein (MBP) by 5.96-fold in the core border region. Controversially, expression of MBP could likely indicate survival of mature myelin as previous studies with NRG-1 treatment have shown, or presentation of the MBP antigen to promote an adaptive immune response (Xu 2012; Alizadeh et al. 2017; Gauthier et al. 2013; Becker et al. 2011; Zierath 2015). Notably, there was also a reduction of SPP1 expression, a marker of disease-related microglia, from 26.39-fold in MCAO to 15.79-fold with NRG-1 treatment. This data suggests that delayed NRG-1 treatment can still have a significant

immunomodulatory effect, potentially priming the core border and peri-infarct region immune cells toward a anti-inflammatory and neuroregenerative environment by restoring microglial mitochondrial activity and removing neurotoxic debris via phagocytosis.

Further analysis into neurodegenerative proteins that are recognized to be associated with ischemia prevalence and later neurodegeneration that were defined within Chapter 3 indicates BACE1, APP, and αβ 1-42 expression are regulated by a positive feedback loop between γ- and β-secretase cleavages on APP as ischemic hypoxic damage continues (Li 2009; Wang 2006). This pattern was defined within the core border region in MCAO and appears to be unchanged with NRG-1 treatment. With BACE1 activity at 4.18-fold with MCAO and 4.09-fold with NRG-1 treatment, APP activity at 5.41-fold with MCAO and 4.95-fold with NRG-1 treatment, and αβ 1-42 deposits at 5.82-fold with MCAO and slightly increased to 7.40-fold with NRG-1 treatment. There also was no difference between groups in ApoE protein expression in the core border, with 6.02-fold increase in MCAO and 6.71-fold increase with NRG-1 treatment. However, phosphotau-S199 protein levels were increased within the core border and peri-infarct regions with NRG-1 treatment. With tau-S199 in the core border upregulated by 57.42-fold with MCAO and 89.94-fold with NRG-1 treatment and upregulated in the peri-infarct by 21.41-fold with MCAO and 43.47-fold with NRG-1 treatment. Phosphorylated tau-proteins hold a complex function, especially after ischemia, as their function is mostly studied in neurodegenerative disorders and recent studies argue that their phosphorylation location after acute injuries may hold a neuroprotective role (Wen 2004; Li 2007a). Phospho-tau S199 upregulation has been linked to neuroprotection, allowing neurons to resist apoptosis in relation to autophagy (Li 2007a). Thus, NRG-1 treatment significantly upregulating this phosphorylation site of phospho-tau in conjunction with promotion of autophagy suggests that NRG-1 is promoting late neuroprotective effects in both the core border and peri-infarct regions.

Table 4.2 Delayed NRG-1 Treatment Induces a Late Neuroprotective and Early Regenerative Profile 3-Days After Ischemic Stroke. Proteins were compared in each respective treatment group against the contralateral side for significant fold changes via an LMM for each ROI including, ipsilateral core border, ipsilateral peri-infarct, and ipsilateral PiNT. Significantly differentially regulated proteins for NRG-1 treated samples are documented for each ROI comparative to MCAO fold changes found from Table 3.2. Upregulated proteins expressed in yellow-green, downregulated proteins expressed in orange-red ($p<0.05$, MCAO (n=3) and MCAO+NRG-1 (n=4)).

		MCAO Core Border	NRG-1 Core Border	MCAO Peri-infarct	NRG-1 Peri-infarct	MCAO PiNT	NRG-1 PiNT
	Significantly changed Proteins	27	37	3	6	1	2
	Upregulated	19	33	3	6	1	2
	Downregulated	8	4	0	0	0	0
Protein Name		Fold Change	Fold Change	Fold Change	Fold Change	Fold Change	Fold Change
Microtubule associated protein 2	MAP2	-7.19	-6.88				
Neuronal nuclei	NeuN	-3.07	-2.20				
Synaptophysin	SYP		2.10				
Vimentin	Vimentin	-2.15					
Aldehyde dehydrogenase 1 family member A1	Aldh1l1	-2.30			2.32		1.59
Glial fibrillary acidic protein	GFAP			23.69	29.97	6.09	5.36
BAG family molecular chaperone regulator 3	BAG3	12.04	12.71	2.96	4.52		
Transcription factor EB	TFEB	2.96	3.27				
Cathepsin D	Ctsd	8.44	9.97				
Unc-51 like autophagy activating kinase 1	ULK1		1.99				
Microtubule-associated protein light chain 3B	LC3B		1.58				
Autophagy related 5	ATG5		2.15				
PTEN-induced kinase 1	PINK1		2.73				
Parkinson Disease 7	Park7		1.95				
Ionized calcium binding adaptor molecule 1	IBA1	4.31	4.57				
Cluster of differentiation molecule 11B	CD11b	8.24	9.02				
Cluster of differentiation 45	CD45	2.25	2.40				
MER proto-oncogene, tyrosine kinase	Mertk		2.68				
Cluster of differentiation 39	CD39	8.74	5.26				
Macrophage scavenger receptor 1	MSR1 (cd204)	9.69	8.15		1.85		
Cluster of differentiation 9	CD9		2.58				
Colony stimulating factor 1 receptor	CSF1R (CD115)		2.13				
Major histocompatibility complex II	MHC II		1.49				
Myelin basic protein	MBP		5.96				
Secreted phosphoprotein 1	SPP1	26.39	15.79				
Marker of proliferation Ki-67	Ki-67				2.48		
Beta-secretase 1	BACE1	4.18	4.09				
Amyloid Precursor Protein	APP	5.41	4.95				
Amyloid-Beta 1-42	αβ 1-42	5.82	7.40				
Apolipoprotein E	ApoE	6.02	6.71				
Phospho-Tau (S199)	tau-S199	57.42	89.94	21.41	43.47		

4.4 Discussion

As we described in Chapter 3, MCAO induces a unique spatial profile with the ischemic core border relating to increased expression of neuronal death, apoptosis, immunoreactivity, and early degeneration. Here our novel findings suggest that delayed daily NRG-1 treatment beginning 24 hours after ischemia can induce a late neuroprotective and early regenerative proteomic profile within the ischemic core border and peri-infarct region as early as three days post-ischemia. Our data suggests that NRG-1 treatment can alter the MCAO proteomic profile by inducing autophagy and mitophagy in neurons and microglia, immune cell phagocytosis, and synaptic activity to

enhance neuroprotection via resistance to apoptosis and priming of a neuroregenerative niche after ischemia.

Our immunohistochemical results demonstrated no difference between MCAO+Vehicle and MCAO+NRG-1 treatment groups, which was consistent with our DSP proteomic results. We found no difference in neuronal death markers, Iba-1, or GFAP expression between treatment groups in DSP proteomic panel results. Taken together, this suggests that traditional immunohistochemical methods are lengthy, expensive, and require large animal numbers in order to determine differences between treatment groups when differences may be molecular, especially with a delayed treatment model as we present here. Utilizing the DSP proteomic panel technology has allowed us to further elucidate a novel mechanism that delayed NRG-1 treatment acts after ischemic stroke in a spatial manner.

NRG-1 treatment resulted in upregulation of many proteins related to autophagy and mitophagy. Importantly, it has been shown that ischemia induces an upregulation in autophagic markers, leading to an increase in neuronal death (Adhami 2007; Wen 2008). However, it has since been elucidated that the specific cell-types expressing autophagy and the success of autophagic flux post-ischemia is critical as enhancing autophagic flux and cell-specific autophagy is largely neuroprotective (Xu 2021; Jeong 2015; Wang 2012). Neuroprotection post-ischemia via enhanced autophagic flux in microglia and neurons has been demonstrated through mediation of the alpha7 nicotinic acetylcholine receptors (Xu 2021; Jeong 2015). In an experimental autoimmune encephalomyelitis model, microglia autophagic flux was inhibited with a ATG5 siRNA and resulted in enhanced neuroinflammation, demonstrating that enhanced microglial autophagy via ATG5 suppresses neuroinflammation with mediation of the alpha7 nicotinic acetylcholine receptors (Shao 2017). NRG-1 has also been shown to mediate an anti-inflammatory effect via upregulating alpha7 nicotinic acetylcholine receptors on microglia *in vitro* (Mencel 2013).

Therefore, autophagic flux is critical not only to neuronal resistance to apoptosis, but microglial mediation of neuroinflammation post-ischemia, and we suggest that NRG-1 treatment is modulating neuroinflammation via autophagic flux in microglia and neuronal resistance to apoptosis via autophagy.

Mitophagy is a selective autophagy process that can be induced by reactive oxygen species or nitrogen starvation and is a key process that involves sequestration and degradation of damaged, defective, or excessive mitochondria (Klionsky 2016). PINK1 is a significant protein of the mitophagy pathway as it accumulates in response to certain forms of mitochondrial damage and is required to successfully sequester mitochondrial fragments for degradation (Klionsky 2016). Mice lacking autophagy in myeloid lineage cells, defined as a deficiency in ATG5, displayed higher expression levels of proinflammatory cytokines without an effect on Iba1 expression (Kotoda. 2018). Additionally, macrophages with restored mitochondrial function after ischemia demonstrated higher plasticity to repolarize to an M2-like phenotype (Van den Bossche 2016). Thus, in addition to the main autophagic pathway, we also suggest that NRG-1 treatment is promoting mitophagy of defective mitochondria in microglia and macrophages within the core border region to prime for an anti-inflammatory state.

NRG-1 treatment also demonstrated an increase in the CSF1 receptor, which has been shown to be upregulated after ischemia in microglia and neurons (Wang 1999). When expressed on monocytes/macrophages it can also be associated with phagocytic capacity as well as proliferation (Jenkins 2013). Microglia and neurons stimulated by CSF1 released by astrocytes promotes survival and microglial response to injury after ischemia (Wang 1999). Additionally, the MSR1 receptor has been associated with resolution of inflammation, clearance of DAMPS, and phagocytosis (Zou 2021; Shichita 2017). SPP1 holds a controversial function after ischemia that involves mediating inflammation via microglia and macrophages (Meller 2005). SPP1 has been

demonstrated to be more upregulated in aged microglia after ischemia and is associated both with acute inflammation and neurodegeneration, although its specific role has yet to be elucidated (Jiang 2020; Sousa 2018). Taken together, we propose that NRG-1 treatment has altered the post-ischemic profile toward a microglial and macrophage mediated response within the core border and peri-infarct region to shift the inflammatory response toward an anti-inflammatory profile to promote survival and neuroregeneration.

Lastly, after ischemic stroke, it has been shown that tau-proteins slowly hyperphosphorylate and accumulate and it has been suggested that the accumulation of phosphorylated tau-proteins contribute to the apoptotic process of neurons (Wen 2004; Zheng 2010). Microglial and oligodendroglial cells have also been found to contain phosphorylated tau-protein accumulations post-ischemia as well (Uchihara 2000). Contrary to expectations, NRG-1 treatment demonstrated a significant increase in phosphorylated tau-S199 deposits in both the core border and peri-infarct regions. An *in vitro* study demonstrated that overexpression of phosphorylated tau at the site S199 can provide acute antiapoptotic effects, but without clearance can lead to later neurodegeneration (Li 2007a). This suggests that overexpression of tau-S199 in combination with enhanced autophagic flux with NRG-1 treatment is providing a mechanism of late neuroprotection for neurons, microglia, and potentially oligodendrocytes as well.

NRG-1 is recognized to act through its ErbB4 receptor, expressed on neurons and glia in the central nervous system (Buonanno 2001). The ErbB4 receptor is enriched at the postsynaptic density and directly associates with PSD-95 as a role in synaptic transmission and neurite outgrowth (Huang 2000; Buonanno 2001; Gerecke 2003). A study that administered NRG-1 (GGF2/neuregulin 1β3) intravenously daily for ten days resulted in increased neural plasticity markers GAP-43 and synaptophysin in the ipsilateral and contralateral somatosensory and motor cortices (Iaci 2016). Additionally, a rat SCI model administered NRG-1 intrathecally continuously

for 1-2 weeks and showed enhanced axonal preservation, increased new oligodendrocytes, and attenuated astrogliosis and tissue degeneration (Gauthier 2013). These studies support that NRG-1 treatment has a direct effect on synaptophysin expression and oligodendrocyte survival and differentiation after injury. However, we must consider the expression of MHCII in conjunction with MBP, as this may suggest that MBP may not be suggestive of surviving mature myelin but rather a presenting antigen to initiate an adaptive immune response (Zierath 2015; Becker 2011). Our data suggests that delayed NRG-1 treatment may initiate this effect as early as 3-days after ischemic injury, characterizing a late neuroprotective profile of neurons and oligodendrocytes as well as an early neuroregenerative profile with synaptic communication and oligodendrocyte preservation.

Overall, our data suggests the novel findings that delayed NRG-1 treatment initiates a unique treatment spatial proteomic profile 3-days post ischemia by inducing autophagy and mitophagy in neurons and microglia, immune cell phagocytosis, and synaptic activity to enhance neuroprotection via resistance to apoptosis and priming of an anti-inflammatory and neuroregenerative niche. Ultimately, we present the idea that NRG-1 treatment can continue to provide significant late neuroprotection and early neuroregeneration post-ischemia and should continue to be studied in spatiotemporal detail at all phases of treatment.

Chapter 5: Conclusion and Overall Discussion

Minutes to hours after ischemia, acute neuroprotection is largely targeted by preventing infarct core expansion into the penumbra via early onset neuronal death. Acute ischemic mechanisms are well-characterized and consist of excitotoxicity, oxidative stress, inflammation, and progression of neuronal death (Dirnagl 1999; Barone 1999; Stoll 1998; del zoppo 2000;

Iadecola 2001, 2011). However, nearly 100+ clinical trials of neuroprotective compounds targeting these mechanisms, including glutamate antagonists, anti-inflammatory compounds, and free radical scavenging agents have failed to demonstrate efficacy in clinical trials with human patients following stroke (Kidwell 2001; O'Collins 2006). Therefore, it has become even more critical to identify a multiple mechanistic treatment with potential to increase the therapeutic treatment window after ischemia.

NRG-1 has demonstrated promise as an acute neuroprotective, anti-inflammatory, and neuroregenerative agent in animal stroke models. These effects have been seen in multiple cerebral injury models, multiple administration methods, and in multiple clinically relevant doses. However, the spatial cellular and inflammatory mechanisms occurring early after ischemic stroke and with NRG-1 treatment had yet to be elucidated. Within these studies we suggest that ischemic stroke initiates unique spatial mechanisms and that NRG-1 treatment targets neuroprotective and neuroregenerative mechanisms within a similar spatial manner with potential of extending the ischemic therapeutic window.

First, we further investigated the clinical potential of NRG-1 as an acute neuroprotectant early after ischemia. Exogenous NRG-1 treatment administered to male and female mice via intra-arterial or intravenous routes significantly reduced cerebral cortical infarct volume, inhibited neuronal injury when measured by FluoroJade B and NeuN labeling, and reduced apoptosis as measured by TUNEL labeling at 24-hours after MCAO. As the NRG-1 receptor, ErbB4, is upregulated in injured neurons and has been suggested to increase the capacity to respond to available NRG-1, neuroprotection by endogenous NRG-1 was investigated in male and female heterozygous knock-out mice (NRG-1 +/1) and WT littermates (Xu 2005; Clement 2007). NRG-1 +/- mice demonstrated a six-times increase in cortical infarct compared to WT littermates at 24-hours post-MCAO. These results suggest that exogenous and endogenous NRG-1 play a critical

role in early neuroprotective mechanisms after ischemia in both male and female mice. Additionally, successful neuroprotection with intravenous exogenous NRG-1 administration suggests a strong potential for clinical success as NRG-1 treatment could be administered in conjunction with tPA.

Next, we utilized immunohistochemistry and Nanostring Digital Spatial Profiling (DSP) to understand the cellular and inflammatory mechanisms occurring early after ischemic stroke in a spatial manner and determine if NRG-1 plays a potential multiple mechanistic role in a similar spatial manner that could be crucial for preclinical and clinical success. Ischemic proteomic spatial profiles were analyzed in regions of interest including the ischemic core border, peri-infarct, and PiNT at 3- days post-ischemia. We demonstrated that the ipsilateral hemisphere initiates unique proteomic regulatory profiles in a spatial manner that can be identified consistently with the immunohistological markers, FJB, GFAP, and Iba-1. Additionally, the core border region presents a unique profile that represents neuronal death, apoptosis, immunoreactivity, and early degeneration. The peri-infarct region demonstrates astrocytic immunoreactivity, apoptosis, and a neurodegenerative proteomic profile, while the PiNT region resulted in an astrocytic immunoreactivity proteomic profile. We demonstrate that the ability to isolate and compare the proteomic profiles of each region has allowed us to determine that each region demonstrates a unique differentially regulated proteomic profile and that substantial loss of data that can occur when the ipsilateral hemisphere is analyzed together.

After characterizing the importance of spatial analysis, we then wanted to investigate whether a treatment spatial proteomic profile could also be elucidated with delayed NRG-1 treatment. Ischemic proteomic spatial profiles were analyzed in the same regions of interest at 3-days post-ischemia after daily NRG-1 treatment beginning at 24-hours after ischemic onset. First, our immunohistochemical results demonstrated no difference between MCAO+Vehicle and

MCAO+NRG-1 treatment groups, which was consistent with our DSP proteomic results. We found no difference in neuronal death markers, Iba-1, or GFAP expression between treatment groups in DSP proteomic panel results. This suggested that elucidating mechanisms for delayed treatment model in ischemia may require more in-depth molecular analysis models rather than gross cellular analysis provided by immunohistochemical markers, of which the DSP proteomic panel provides. Our novel findings suggest that delayed daily NRG-1 treatment beginning 24 hours after ischemia can induce a late neuroprotective and early regenerative proteomic profile within the ischemic core border region and peri-infarct region as early as three days post-ischemia. Our data suggests that NRG-1 treatment can alter the ischemic proteomic profile by inducing autophagy and mitophagy in neurons and microglia, immune cell phagocytosis, and synaptic activity to enhance neuroprotection via resistance to apoptosis and priming of a neuroregenerative niche after ischemia.

Overall, our data highlight the importance of identifying ischemic spatial mechanisms in order to understand the complex, dynamic interactions throughout ischemic progression and repair as well to introduce a successful ischemic therapeutic. We identify NRG-1 as a potent ischemic therapeutic capable of inducing immediate and late neuroprotection, early neuroregeneration, and extending the therapeutic treatment window after ischemia.

Bibliography and References

Adhami, F., A. Schloemer & C. Y. Kuan (2007) The roles of autophagy in cerebral ischemia. Autophagy, 3, 42-4.

Albers, G. W., L. B. Goldstein, D. C. Hess, L. R. Wechsler, K. L. Furie, P. B. Gorelick, P. Hurn, D. S. Liebeskind, R. G. Nogueira & J. L. Saver (2011) Stroke Treatment Academic Industry Roundtable (STAIR) Recommendations for Maximizing the Use of Intravenous Thrombolytics and Expanding Treatment Options With Intra-arterial and Neuroprotective Therapies. Stroke, 42, 2645-2650.

Alizadeh, A., S. M. Dyck, H. Kataria, G. M. Shahriary, D. H. Nguyen, K. T. Santhosh & S. Karimi-Abdolrezaee (2017) Neuregulin-1 positively modulates glial response and improves neurological recovery following traumatic spinal cord injury. Glia, 65, 1152-1175.

Alkayed NJ, Harukuni I, Kimes AS, London ED, Traystman RJ, Hurn PD (1998) Gender-linked brain injury in experimental stroke. Stroke 29:159–165 discussion 166.

Antonioli, L., P. Pacher, E. S. Vizi & G. Haskó (2013) CD39 and CD73 in immunity and inflammation. Trends Mol Med, 19, 355-67.

Baek, A. E., N. R. Sutton, D. Petrovic-Djergovic, H. Liao, J. J. Ray, J. Park, Y. Kanthi & D. J. Pinsky (2017) Ischemic Cerebroprotection Conferred by Myeloid Lineage-Restricted or Global CD39 Transgene Expression. Circulation, 135, 2389-2402.

Barber PA, Hoyte L, Colbourne F, Buchan AM (2004) Temperature regulated model of focal ischemia in the mouse: a study with histopathological and behavioral outcomes. Stroke 35:1720–1725.

Barone FC & Feuerstein GZ (1999) Inflammatory mediators and stroke: new opportunities for novel therapeutics. J Cereb Blood Flow Metab 19(8):819-834.

Barres, B. A. & M. C. Raff (1999) Axonal control of oligodendrocyte development. Journal of Cell Biology, 147, 1123-1128.

Becker, K. J., A. J. Kalil, P. Tanzi, D. K. Zierath, A. V. Savos, J. M. Gee, J. Hadwin, K. T. Carter, D. Shibata & K. C. Cain (2011) Autoimmune responses to the brain after stroke are associated with worse outcome. Stroke, 42, 2763-9.

Benjamin (2017) Heart Disease and Stroke Statistics-2017 Update: A Report From the American Heart Association (vol 135, pg e146, 2017). Circulation, 136, E196-E196.

Buonanno, A. & G. D. Fischbach (2001) Neuregulin and ErbB receptor signaling pathways in the nervous system. Current Opinion in Neurobiology, 11, 287-296.

Carmichael, Thomas S. (2006) Cellular and Molecular Mechanisms of Neural Repair after Stroke: Making Waves. Ann Neurol, 59: 735-742.

Choi, I. A., J. H. Yun, J. H. Kim, H. Y. Kim, D. H. Choi & J. Lee (2019) Sequential Transcriptome Changes in the Penumbra after Ischemic Stroke. Int J Mol Sci, 20.

Clement, C. M., L. K. Thomas, Y. Mou, D. R. Croslan, G. H. Gibbons & B. D. Ford (2007) Neuregulin-1 attenuates neointimal formation following vascular injury and inhibits the proliferation of vascular smooth muscle cells. Journal of Vascular Research, 44, 303-312.

Cramer, S.C. (2004) Functional Imaging in Stroke Recovery. Stroke 35: 2695-2698.

Cramer, S.C., Shah, R., Juranek, J., Crafton, K.R., and Le, V. (2006a) Activity in the Peri-Infarct Rim in Relation to Recovery from Stroke. Stroke 37: 111-115.

Cramer, S.C., and Crafton, K.R. (2006b) Somatotopy and Movement Representation Sites Following Cortical Stroke. Exp Brain Res 168: 25-32.

Davies, C. A., S. A. Loddick, R. P. Stroemer, J. Hunt & N. J. Rothwell (1998) An integrated analysis of the progression of cell responses induced by permanent focal middle cerebral artery occlusion in the rat. Exp Neurol, 154, 199-212.

del Zoppo G, et al. (2000) Inflammation and stroke: putative role for cytokines, adhesion molecules and iNOS in brain response to ischemia. Brain Pathol 10(1):95-112.

Detante, O., A. Jaillard, A. Moisan, M. Barbieux, I. M. Favre, K. Garambois, M. Hommel & C. Remy (2014) Biotherapies in stroke. Rev Neurol (Paris), 170, 779-98.

Dirnagl U, Iadecola C, & Moskowitz MA (1999) Pathobiology of ischaemic stroke: an integrated view. Trends Neurosci 22(9):391-397.

Eilam, R., R. Pinkas-Kramarski, B. J. Ratzkin, M. Segal & Y. Yarden (1998) Activity-dependent regulation of Neu differentiation factor neuregulin expression in rat brain. Proceedings of the National Academy of Sciences of the United States of America, 95, 1888-1893.

Erickson SL, KSOS, Ghaboosi N, Loverro L, Frantz G, Bauer M, Lu LH, Moore MW (1997) ErbB3 is required for normal cerebellar and cardiac development: a comparison with ErbB2-and heregulin-deficient mice. Development 124:4999–5011.

Falls DL, Rosen KM, Corfas G, Lane WS, Fischbach GD(1993) ARIA, a protein that stimulates acetylcholine receptor synthesis, is a member of the neu ligand family. Cell 72:801–815.

Fisher M, Feuerstein G, Howells DW, Hurn PD, Kent TA, Savitz SI, Lo EH (2009) Update of the stroke therapy academic industry roundtable preclinical recommendations. Stroke 40:2244–2250.

Fitch, M. T., C. Doller, C. K. Combs, G. E. Landreth & J. Silver (1999) Cellular and molecular mechanisms of glial scarring and progressive cavitation: in vivo and in vitro analysis of inflammation-induced secondary injury after CNS trauma. J Neurosci, 19, 8182-98.

Fricker, F. R. & D. L. Bennett (2011a) The role of neuregulin-1 in the response to nerve injury. Future Neurology, 6, 809-822.

Fricker, F. R., N. Lago, S. Balarajah, C. Tsantoulas, S. Tanna, N. Zhu, S. K. Fageiry, M. Jenkins, A. N. Garratt, C. Birchmeier & D. L. H. Bennett (2011b) Axonally Derived Neuregulin-1 Is Required for Remyelination and Regeneration after Nerve Injury in Adulthood. Journal of Neuroscience, 31, 3225-3233.

Gao R, Zhang J, Cheng L,Wu X, Dong W, Yang X, Li T, Liu X, Xu Y, Li X et al (2010) A phase II, randomized, double-blind, multicenter, based on standard therapy, placebo-controlled study of the efficacy and safety of recombinant human neuregulin-1 in patients with chronic heart failure. J Am Coll Cardiol 55:1907–1914.

Gao, G., C. Li, J. Zhu, Y. Wang, Y. Huang, S. Zhao, S. Sheng, Y. Song, C. Ji, X. Yang, L. Ye, X. Qi, Y. Zhang, X. Xia & J. C. Zheng (2020) Glutaminase 1 Regulates Neuroinflammation After Cerebral Ischemia Through Enhancing Microglial Activation and Pro-Inflammatory Exosome Release. Front Immunol, 11, 161.

Gauthier, M. K., K. Kosciuczyk, L. Tapley & S. Karimi-Abdolrezaee (2013) Dysregulation of the neuregulin-1-ErbB network modulates endogenous oligodendrocyte differentiation and preservation after spinal cord injury. European Journal of Neuroscience, 38, 2693-2715.

Gerecke, K. M., S. L. Carroll, S. Roysommuti & J. M. Wyss (2003) THE ROLE OF NEUREGULIN-1β IN THE MATURE CENTRAL NERVOUS SYSTEM. Thai Journal of Physiological Sciences, 16.

Gerlai R, Pisacane P, Erickson S (2000) Heregulin, but not ErbB2 or ErbB3, heterozygous mutant mice exhibit hyperactivity in multiple behavioral tasks. Behav Brain Res 109:219–227.

Giulian, D., M. Corpuz, S. Chapman, M. Mansouri & C. Robertson (1993a) Reactive mononuclear phagocytes release neurotoxins after ischemic and traumatic injury to the central nervous system. J Neurosci Res, 36, 681-93.

Giulian, D., K. Vaca & M. Corpuz (1993b) Brain glia release factors with opposing actions upon neuronal survival. J Neurosci, 13, 29-37.

Guan YF, Wu CY, Fang YY, Zeng YN, Luo ZY, Li SJ, Li XW, Zhu XH, Mei L, Gao TM(2015) Neuregulin 1 protects against ischemic brain injury via ErbB4 receptors by increasing GABAergic transmission. Neuroscience 307:151–159.

Guglielmotto, M., M. Aragno, R. Autelli, L. Giliberto, E. Novo, S. Colombatto, O. Danni, M. Parola, M. A. Smith, G. Perry, E. Tamagno & M. Tabaton (2009) The up-regulation of BACE1 mediated by hypoxia and ischemic injury: role of oxidative stress and HIF1alpha. J Neurochem, 108, 1045-56.

Guo WP, Wang J, Li RX, Peng YW. Neuroprotective effects of neuregulin-1 in rat models of focal cerebral ischemia. Brain Res. 2006;1087(1):180-5. PubMed PMID: 16616052.

Hallenbeck, J. M. (1996) Significance of the inflammatory response in brain ischemia. Acta Neurochir Suppl, 66, 27-31.

Ho WH, Armanini MP, Nuijens A, Phillips HS, Osheroff PL (1995) Sensory and motor neuron-derived factor. A novel heregulin variant highly expressed in sensory and motor neurons. J Biol Chem 270: 26722.

Holmes WE, Sliwkowski MX, Akita RW, Henzel WJ, Lee J, Park JW, Yansura D, Abadi N, Raab H, Lewis GD et al (1992) Identification of heregulin, a specific activator of p185erbB2. Science 256:1205–1210.

Huang, Y. Z., S. Won, D. W. Ali, Q. Wang, M. Tanowitz, Q. S. Du, K. A. Pelkey, D. J. Yang, W. C. Xiong, M. W. Salter & L. Mei (2000) Regulation of neuregulin signaling by PSD-95 interacting with ErbB4 at CNS synapses. Neuron, 26, 443-55.

Huang, S., X. Ge, J. Yu, Z. Han, Z. Yin, Y. Li, F. Chen, H. Wang, J. Zhang & P. Lei (2018) Increased miR-124-3p in microglial exosomes following traumatic brain injury inhibits neuronal inflammation and contributes to neurite outgrowth. FASEB J, 32, 512-528.

Hyman, M. C., D. Petrovic-Djergovic, S. H. Visovatti, H. Liao, S. Yanamadala, D. Bouïs, E. J. Su, D. A. Lawrence, M. J. Broekman, A. J. Marcus & D. J. Pinsky (2009) Self-regulation of inflammatory cell trafficking in mice by the leukocyte surface apyrase CD39. J Clin Invest, 119, 1136-49.

Iaci JF, Ganguly A, Finklestein SP, Parry TJ, Ren J, Saha S, Sietsma DK, Srinivas M, Vecchione AM, Caggiano AO (2010) Glial growth factor 2 promotes functional recovery with treatment initiated up to 7 days after permanent focal ischemic stroke. Neuropharmacology 59: 640–649.

Iaci, J. F., T. J. Parry, Z. Huang, E. Pavlopoulos, S. P. Finklestein, J. Ren & A. Caggiano (2016) An optimized dosing regimen of cimaglermin (neuregulin 1β3, glial growth factor 2) enhances molecular markers of neuroplasticity and functional recovery after permanent ischemic stroke in rats. Journal of Neuroscience Research, 94, 253-265.

Iadecola C & Alexander M (2001) Cerebral ischemia and inflammation. Curr Opin Neurol 14(1):89-94.

Iadecola C & Anrather J (2011) The immunology of stroke: from mechanisms to translation. Nat Med 17(7):796-808.

Ito, D., K. Tanaka, S. Suzuki, T. Dembo & Y. Fukuuchi (2001) Enhanced expression of Iba1, ionized calcium-binding adapter molecule 1, after transient focal cerebral ischemia in rat brain. Stroke, 32, 1208-15.

Jabbour A, Hayward CS, Keogh AM, Kotlyar E, McCrohon JA, England JF, Amor R, Liu X, Li XY, Zhou MD et al (2011) Parenteral administration of recombinant human neuregulin-1 to patients with stable chronic heart failure produces favourable acute and chronic haemodynamic responses. Eur J Heart Fail 13:83–92.

Jayaraj, R. L., S. Azimullah, R. Beiram, F. Y. Jalal & G. A. Rosenberg (2019) Neuroinflammation: friend and foe for ischemic stroke. J Neuroinflammation, 16, 142.

Jenkins, S. J., D. Ruckerl, G. D. Thomas, J. P. Hewitson, S. Duncan, F. Brombacher, R. M. Maizels, D. A. Hume & J. E. Allen (2013) IL-4 directly signals tissue-resident macrophages to proliferate beyond homeostatic levels controlled by CSF-1. J Exp Med, 210, 2477-91.

Jeong, H. K., K. Ji, K. Min & E. H. Joe (2013) Brain inflammation and microglia: facts and misconceptions. Exp Neurobiol, 22, 59-67.

Jeong, J. K. & S. Y. Park (2015) Melatonin regulates the autophagic flux via activation of alpha-7 nicotinic acetylcholine receptors. J Pineal Res, 59, 24-37.

Jiang, L., H. Mu, F. Xu, D. Xie, W. Su, J. Xu, Z. Sun, S. Liu, J. Luo, Y. Shi, R. K. Leak, L. R. Wechsler, J. Chen & X. Hu (2020) Transcriptomic and functional studies reveal undermined chemotactic and angiostimulatory properties of aged microglia during stroke recovery. J Cereb Blood Flow Metab, 40, S81-S97.

Jovin, T. G., G. W. Albers & D. S. Liebeskind (2016) Stroke Treatment Academic Industry Roundtable: The Next Generation of Endovascular Trials. Stroke, 47.

Kawabori, M. & M. A. Yenari (2015) The role of the microglia in acute CNS injury. Metab Brain Dis, 30, 381-92.

Kidwell, C. S., D. S. Liebeskind, S. Starkman & J. L. Saver (2001) Trends in acute ischemic stroke trials through the 20th century. Stroke, 32, 1349-59.

Kim, J. Y., J. Park, J. Y. Chang, S. H. Kim & J. E. Lee (2016) Inflammation after Ischemic Stroke: The Role of Leukocytes and Glial Cells. Exp Neurobiol, 25, 241-251.

Kindy, M. S., A. N. Bhat & N. R. Bhat (1992) Transient ischemia stimulates glial fibrillary acid protein and vimentin gene expression in the gerbil neocortex, striatum and hippocampus. Brain Res Mol Brain Res, 13, 199-206.

Klionsky, D. J., K. Abdelmohsen, A. Abe, M. J. Abedin, H. Abeliovich, A. Acevedo Arozena, H. Adachi, C. M. Adams, P. D. Adams, K. Adeli, P. J. Adhihetty, S. G. Adler, G. Agam, R. Agarwal, M. K. Aghi, M. Agnello, P. Agostinis, P. V. Aguilar, J. Aguirre-Ghiso, E. M. Airoldi, S. Ait-Si-Ali, T. Akematsu, E. T. Akporiaye, M. Al-Rubeai, G. M. Albaiceta, C. Albanese, D. Albani, M. L. Albert, J. Aldudo, H. Algül, M. Alirezaei, I. Alloza, A. Almasan, M. Almonte-Beceril, E. S. Alnemri, C. Alonso, N. Altan-Bonnet, D. C. Altieri, S. Alvarez, L. Alvarez-Erviti, S. Alves, G. Amadoro, A. Amano, C. Amantini, S. Ambrosio, I. Amelio, A. O. Amer, M. Amessou, A. Amon, Z. An, F. A. Anania, S. U. Andersen, U. P. Andley, C. K. Andreadi, N. Andrieu-Abadie, A. Anel, D. K. Ann, S. Anoopkumar-Dukie, M. Antonioli, H. Aoki, N. Apostolova, S. Aquila, K. Aquilano, K. Araki, E. Arama, A. Aranda, J. Araya, A. Arcaro, E. Arias, H. Arimoto, A. R. Ariosa, J. L. Armstrong, T. Arnould, I. Arsov, K. Asanuma, V. Askanas, E. Asselin, R. Atarashi, S. S. Atherton, J. D. Atkin, L. D. Attardi, P. Auberger, G. Auburger, L. Aurelian, R. Autelli, L. Avagliano, M. L. Avantaggiati, L. Avrahami, S. Awale, N. Azad, T. Bachetti, J. M. Backer, D. H. Bae, J. S. Bae, O. N. Bae, S. H. Bae, E. H. Baehrecke, S. H. Baek, S. Baghdiguian, A. Bagniewska-Zadworna, et al. (2016) Guidelines for the use and interpretation of assays for monitoring autophagy (3rd edition). Autophagy, 12, 1-222.

Koistinaho, M. & J. Koistinaho (2005) Interactions between Alzheimer's disease and cerebral ischemia--focus on inflammation. Brain Res Brain Res Rev, 48, 240-50.

Kotoda, M., H. Furukawa, T. Miyamoto, M. Korai, F. Shikata, A. Kuwabara, X. Xiong, C. Rutledge, R. G. Giffard & T. Hashimoto (2018) Role of Myeloid Lineage Cell Autophagy in Ischemic Brain Injury. Stroke, 49, 1488-1495.

Lapchak, P. A., J. H. Zhang & L. J. Noble-Haeusslein (2013) RIGOR Guidelines: Escalating STAIR and STEPS for Effective Translational Research. Translational Stroke Research, 4, 279-285.

Li, H. L., H. H. Wang, S. J. Liu, Y. Q. Deng, Y. J. Zhang, Q. Tian, X. C. Wang, X. Q. Chen, Y. Yang, J. Y. Zhang, Q. Wang, H. Xu, F. F. Liao & J. Z. Wang (2007a) Phosphorylation of tau antagonizes apoptosis by stabilizing beta-catenin, a mechanism involved in Alzheimer's neurodegeneration. Proc Natl Acad Sci U S A, 104, 3591-6.

Li, Y., Z. Xu, G. D. Ford, D. R. Croslan, T. Cairobe, Z. Li & B. D. Ford (2007b) Neuroprotection by neuregulin-1 in a rat model of permanent focal cerebral ischemia. Brain Res, 1184, 277-83.

Li, Q., Z. Li, Y. W. Mei & Y. H. Guo (2008) Neuregulin attenuated cerebral ischemia-Creperfusion injury via inhibiting apoptosis and upregulating aquaporin-4. Neuroscience Letters, 443, 155-159.

Li, L., X. Zhang, D. Yang, G. Luo, S. Chen & W. Le (2009) Hypoxia increases Abeta generation by altering beta- and gamma-cleavage of APP. Neurobiol Aging, 30, 1091-8.

Li, S. L., J. J. Overman, D. Katsman, S. V. Kozlov, C. J. Donnelly, J. L. Twiss, R. J. Giger, G. Coppola, D. H. Geschwind & S. T. Carmichael (2010) An age-related sprouting transcriptome provides molecular control of axonal sprouting after stroke. Nature Neuroscience, 13, 1496-U82.

Li C-X, Kempf DJ, Tong FC, Yan Y, Xu Z, Connor-Stroud FR, Ford BD, Howell LL, Zhang X (2018) Longitudinal MRI evaluation of ischemic stroke in the basal ganglia of a rhesus macaque (Macaca mullata) with seizures. Comp Med 68(6):496–502.

Lipton, Peter (1999) Ischemic Cell Death in Brain Neurons. Physiological Reviews 79(4): 1431-1568.

Liu, Y., X. Xue, H. Zhang, X. Che, J. Luo, P. Wang, J. Xu, Z. Xing, L. Yuan, X. Fu, D. Su, S. Sun, C. Wu & J. Yang (2019) Neuronal-targeted TFEB rescues dysfunction of the autophagy-lysosomal pathway and alleviates ischemic injury in permanent cerebral ischemia. Autophagy, 15, 493-509.

Lloyd-Jones, D., R. J. Adams, T. M. Brown, M. Carnethon, S. Dai, G. De Simone, T. B. Ferguson, E. Ford, K. Furie, C. Gillespie, A. Go, K. Greenlund, N. Haase, S. Hailpern, M. Ho, V. Howard, B. Kissela, S. Kittner, D. Lackland, L. Lisabeth, A. Marelli, M. M. McDermott, J. Meigs, D. Mozaffarian, M. Mussolino, G. Nichol, V. L. Roger, W. Rosamond, R. Sacco, P. Sorlie, R. Stafford, T. Thom, S. Wasserthiel-Smoller, N. Wong & J. Wylie-Rosett (2010) Heart Disease and Stroke Statistics—2010 Update A Report From the American Heart Association. Circulation AHA, 121, e46-e215.

Lok, J., S. Zhao, W. Leung, J. H. Seo, D. Navaratna, X. Wang, M. J. Whalen & E. H. Lo (2012) Neuregulin-1 effects on endothelial and blood-brain-barrier permeability after experimental injury. Transl Stroke Res, 3 Suppl 1, S119-24.

Marchionni MA, Goodearl AD, Chen MS, Bermingham-McDonogh O, Kirk C, Hendricks M, Danehy F, Misumi D, Sudhalter J, Kobayashi K et al (1993) Glial growth factors are alternatively spliced erbB2 ligands expressed in the nervous system. Nature 362:312–318.

Matsumoto, H., Y. Kumon, H. Watanabe, T. Ohnishi, M. Shudou, C. Ii, H. Takahashi, Y. Imai & J. Tanaka (2007) Antibodies to CD11b, CD68, and lectin label neutrophils rather than microglia in traumatic and ischemic brain lesions. J Neurosci Res, 85, 994-1009.

Meller, R., S. L. Stevens, M. Minami, J. A. Cameron, S. King, H. Rosenzweig, K. Doyle, N. S. Lessov, R. P. Simon & M. P. Stenzel-Poore (2005) Neuroprotection by osteopontin in stroke. J Cereb Blood Flow Metab, 25, 217-25.

Mencel, M., M. Nash & C. Jacobson (2013) Neuregulin Upregulates Microglial [alpha]7 Nicotinic Acetylcholine Receptor Expression in Immortalized Cell Lines: Implications for Regulating Neuroinflammation. PLoS One, 8.

Meyer D, Birchmeier C (1995) Multiple essential functions of neuregulin in development. Nature 378:386–390.

Meyer, D., T. Yamaai, A. Garratt, E. RiethmacherSonnenberg, D. Kane, L. E. Theill & C. Birchmeier (1997) Isoform-specific expression and function of neuregulin. Development, 124, 3575-3586.

Murphy SJ, McCullough LD, Smith JM (2004) Stroke in the female: role of biological sex and estrogen. ILAR J 45:147–159.

Murphy SJ, Kirsch JR, Zhang W, Grafe MR, West GA, del Zoppo GJ, Traystman RJ, Hum PD (2008) Can gender differences be evaluated in a rhesus macaque (Macaca mulatta) model of focal cerebral ischemia? Comp Med 58:588–596.

Navarro-Gonzlez C, Huerga-Gomez A, Fazzari P. Nrg1 Intracellular Signaling Is Neuroprotective upon Stroke. Oxidative Medicine and Cellular Longevity. 2019;2019:15. doi: 10.1155/2019/3930186.

Noll, J. M., Y. Li, T. J. Distel, G. D. Ford & B. D. Ford (2019) Neuroprotection by Exogenous and Endogenous Neuregulin-1 in Mouse Models of Focal Ischemic Stroke. J Mol Neurosci, 69, 333-342.

Nowicka, D., K. Rogozinska, M. Aleksy, O. W. Witte & J. Skangiel-Kramska (2008) Spatiotemporal dynamics of astroglial and microglial responses after photothrombotic stroke in the rat brain. Acta Neurobiol Exp (Wars), 68, 155-68.

O'Collins, V. E., M. R. Macleod, G. A. Donnan, L. L. Horky, B. H. van der Worp & D. W. Howells (2006) 1,026 experimental treatments in acute stroke. Ann Neurol, 59, 467-77.

O'Tuathaigh CM, Babovic D, O'Sullivan GJ, Clifford JJ, Tighe O, Croke DT, Harvey R, Waddington JL (2007) Phenotypic characterization of spatial cognition and social behavior in mice with 'knockout' of the schizophrenia risk gene neuregulin 1. Neuroscience 147:18–27.

O'Tuathaigh CM, O'Connor AM, O'Sullivan GJ, Lai D, Harvey R, Croke DT, Waddington JL (2008) Disruption to social dyadic interactions but not emotional/anxiety-related behaviour in mice with heterozygous 'knockout' of the schizophrenia risk gene neuregulin-1. Prog Neuro-Psychopharmacol Biol Psychiatry 32:462–466.

O'Tuathaigh CM, Harte M, O'Leary C, O'Sullivan GJ, Blau C, Lai D, Harvey RP, Tighe O, Fagan AJ, Kerskens C et al (2010) Schizophrenia-related endophenotypes in heterozygous neuregulin-1 'knockout' mice. Eur J Neurosci 31:349–358.

Parker, M. W., Y. Chen, J. M. Hallenbeck & B. D. Ford (2002) Neuregulin expression after focal stroke in the rat. Neuroscience Letters, 334, 169-172.

Pekny, M. & M. Nilsson (2005) Astrocyte activation and reactive gliosis. Glia, 50, 427-34.

Price, C.J.S., Wang, D., Menon, D.K., Guadagno, J.V., Cleij, M., Fryer, T., Aigbirhio, F., Baron, J.C., and Warburton, E.A. (2006) Intrinsic Activated Microglia Map to the Peri-infarct Zone in the Subacute Phase of Ischemic Stroke. Stroke 37: 1749-1753.

Qian H, Dou Z, Ruan W, He P, Zhang JH, Yan F (2018) ErbB4 preserves blood-brain barrier integrity via the YAP/PIK3CB pathway after subarachnoid hemorrhage in rats. Front Neurosci 12:492.

Rodriguez-Mercado R, Ford GD, Xu Z, Kraiselburd EN, Martinez MI, Eterovic V, Colon E, Rodriguez IV, Portilla P, Ferchmin PA et al (2012) Acute neuronal injury and blood genomic profiles in a nonhuman primate model for ischemic stroke. J Comp Med 62:1–12.

Sanchez-Bezanilla, S., R. J. Hood, L. E. Collins-Praino, R. J. Turner, F. R. Walker, M. Nilsson & L. K. Ong (2021) More than motor impairment: A spatiotemporal analysis of cognitive

impairment and associated neuropathological changes following cortical photothrombotic stroke. J Cereb Blood Flow Metab, 271678X211005877.

Sandrock AW Jr, Dryer SE, Rosen KM, Gozani SN, Kramer R, Theill LE, Fischbach GD (1997) Maintenance of acetylcholine receptor number by neuregulins at the neuromuscular junction in vivo. Science 276:599–603.

Savchenko, V. L., J. A. McKanna, I. R. Nikonenko & G. G. Skibo (2000) Microglia and astrocytes in the adult rat brain: comparative immunocytochemical analysis demonstrates the efficacy of lipocortin 1 immunoreactivity. Neuroscience, 96, 195-203.

Saver, J. L., G. W. Albers, B. Dunn, K. C. Johnston & M. Fisher (2009) Stroke Therapy Academic Industry Roundtable (STAIR) Recommendations For Extended Window Acute Stroke Therapy Trials. Stroke, 40, 2594-2600.

Shao, B. Z., P. Ke, Z. Q. Xu, W. Wei, M. H. Cheng, B. Z. Han, X. W. Chen, D. F. Su & C. Liu (2017) Autophagy Plays an Important Role in Anti-inflammatory Mechanisms Stimulated by Alpha7 Nicotinic Acetylcholine Receptor. Front Immunol, 8, 553.

Shichita, T., M. Ito, R. Morita, K. Komai, Y. Noguchi, H. Ooboshi, R. Koshida, S. Takahashi, T. Kodama & A. Yoshimura (2017) MAFB prevents excess inflammation after ischemic stroke by accelerating clearance of damage signals through MSR1. Nat Med, 23, 723-732.

Shigyo, M. & C. Tohda (2016) Extracellular vimentin is a novel axonal growth facilitator for functional recovery in spinal cord-injured mice. Sci Rep, 6, 28293.

Shyu, W. C., S. Z. Lin, M. F. Chiang, H. I. Yang, P. Thajeb & H. Li (2004) Neuregulin-1 reduces ischemia-induced brain damage in rats. Neurobiology of Aging, 25, 935-944.

Sousa, C., A. Golebiewska, S. K. Poovathingal, T. Kaoma, Y. Pires-Afonso, S. Martina, D. Coowar, F. Azuaje, A. Skupin, R. Balling, K. Biber, S. P. Niclou & A. Michelucci (2018) Single-cell transcriptomics reveals distinct inflammation-induced microglia signatures. EMBO Rep, 19.

Stefansson H, Sigurdsson E, Steinthorsdottir V, Bjornsdottir S, Sigmundsson T, Ghosh S, Brynjolfsson J, Gunnarsdottir S, Ivarsson O, Chou TT et al (2002) Neuregulin 1 and susceptibility to schizophrenia. Am J Hum Genet 71:877–892 Stefansson H, Steinthorsdottir V,

Stoll G, Jander S, & Schroeter M (1998) Inflammation and glial responses in ischemic brain lesions. Prog Neurobiol 56(2):149-171.

Sun, X., G. He, H. Qing, W. Zhou, F. Dobie, F. Cai, M. Staufenbiel, L. E. Huang & W. Song (2006) Hypoxia facilitates Alzheimer's disease pathogenesis by up-regulating BACE1 gene expression. Proc Natl Acad Sci U S A, 103, 18727-32.

Thorgeirsson TE, Gulcher JR, Stefansson K (2004) Neuregulin 1 and schizophrenia. Ann Med 36:62–71.

Tokita, Y., H. Keino, F. Matsui, S. Aono, H. Ishiguro, S. Higashiyama & A. Oohira (2001) Regulation of neuregulin expression in the injured rat brain and cultured astrocytes. Journal of Neuroscience, 21, 1257-1264.

Toung TJ, Chen TY, Littleton-Kearney MT, Hurn PD, Murphy SJ (2004) Effects of combined estrogen and progesterone on brain infarction in reproductively senescent female rats. J Cereb Blood FlowMetab 24: 1160–1166.

Touzani O, Roussel S, & MacKenzie ET (2001) The ischaemic penumbra. Curr Opin Neurol 14(1):83-88.

Uchihara, T., K. Tsuchiya, A. Nakamura & K. Ikeda (2000) Appearance of tau-2 immunoreactivity in glial cells in human brain with cerebral infarction. Neurosci Lett, 286, 99-102.

Van den Bossche, J., J. Baardman, N. A. Otto, S. van der Velden, A. E. Neele, S. M. van den Berg, R. Luque-Martin, H. J. Chen, M. C. Boshuizen, M. Ahmed, M. A. Hoeksema, A. F. de Vos & M. P. de Winther (2016) Mitochondrial Dysfunction Prevents Repolarization of Inflammatory Macrophages. Cell Rep, 17, 684-696.

Wang, Y., O. Berezovska & S. Fedoroff (1999) Expression of colony stimulating factor-1 receptor (CSF-1R) by CNS neurons in mice. J Neurosci Res, 57, 616-32.

Wang, R., Y. W. Zhang, X. Zhang, R. Liu, S. Hong, K. Xia, J. Xia, Z. Zhang & H. Xu (2006) Transcriptional regulation of APH-1A and increased gamma-secretase cleavage of APP and Notch by HIF-1 and hypoxia. FASEB J, 20, 1275-7.

Wang, P., Y. F. Guan, H. Du, Q. W. Zhai, D. F. Su & C. Y. Miao (2012) Induction of autophagy contributes to the neuroprotection of nicotinamide phosphoribosyltransferase in cerebral ischemia. Autophagy, 8, 77-87.

Wang, S., Y. Li, R. Paudyal, B. D. Ford & X. Zhang (2015) Spatio-temporal assessment of the neuroprotective effects of neuregulin-1 on ischemic stroke lesions using MRI. J.Neurol.Sci., 357, 28-34.

Wen D, Peles E, Cupples R, Suggs SV, Bacus SS, Luo Y, Trail G, Hu S, Silbiger SM, Levy RB et al (1992) Neu differentiation factor: a transmembrane glycoprotein containing an EGF domain and an immunoglobulin homology unit. Cell 69:559–572.

Wen, Y., S. Yang, R. Liu & J. W. Simpkins (2004) Transient cerebral ischemia induces site-specific hyperphosphorylation of tau protein. Brain Res, 1022, 30-8.

Wen, Y. D., R. Sheng, L. S. Zhang, R. Han, X. Zhang, X. D. Zhang, F. Han, K. Fukunaga & Z. H. Qin (2008) Neuronal injury in rat model of permanent focal cerebral ischemia is associated with activation of autophagic and lysosomal pathways. Autophagy, 4, 762-9.

Xu Z, Jiang J, Ford G, Ford BD (2004) Neuregulin-1 is neuroprotective and attenuates inflammatory responses induced by ischemic stroke. Biochem Biophys Res Commun 322:440–446.

Xu Z, Croslan DR, Harris AE, Ford GD, Ford BD (2006) Extended therapeutic window and functional recovery after intraarterial administration of neuregulin-1 after focal ischemic stroke. J Cereb Blood Flow Metab 26:527–535.

Xu, C. C., L. Lv, G. L. Zheng, B. Y. Li, L. Gao & Y. Sun (2012) Neuregulin1 beta 1 protects oligodendrocyte progenitor cells from oxygen glucose deprivation injury induced apoptosis via ErbB4-dependent activation of PI3-kinase/Akt. Brain Research, 1467, 104-112.

Xu, Z. Q., J. J. Zhang, N. Kong, G. Y. Zhang, P. Ke, T. Han, D. F. Su & C. Liu (2021) Autophagy is Involved in Neuroprotective Effect of Alpha7 Nicotinic Acetylcholine Receptor on Ischemic Stroke. Front Pharmacol, 12, 676589.

Yan F, Tan X, Wan W, Dixon BJ, Fan R, Enkhjargal B, Li Q, Zhang J, Chen G, Zhang JH (2017) ErbB4 protects against neuronal apoptosis via activation of YAP/PIK3CB signaling pathway in a rat model of subarachnoid hemorrhage. Exp Neurol 297:92–100.

Yanagida, T., Y. Kitamura, K. Yamane, K. Takahashi, K. Takata, D. Yanagisawa, H. Yasui, T. Taniguchi, T. Taira, T. Honda & H. Ariga (2009) Protection against oxidative stress-induced neurodegeneration by a modulator for DJ-1, the wild-type of familial Parkinson's disease-linked PARK7. J Pharmacol Sci, 109, 463-8.

Zagrean, A. M., D. M. Hermann, I. Opris, L. Zagrean & A. Popa-Wagner (2018) Multicellular Crosstalk Between Exosomes and the Neurovascular Unit After Cerebral Ischemia. Therapeutic Implications. Front Neurosci, 12, 811.

Zhang X, Tong F, Li CX, Yan Y, Kempf D, Nair G, Wang S, Muly EC, Zola S, Howell L (2015) Temporal evolution of ischemic lesions in nonhuman primates: a diffusion and perfusion MRI study. PLoS One 10:e0117290.

Zheng, G. Q., X. M. Wang, Y. Wang & X. T. Wang (2010) Tau as a potential novel therapeutic target in ischemic stroke. J Cell Biochem, 109, 26-9.

Zhong J, Chan A, Morad L, Kornblum HI, Fan G, Carmichael ST (2010) Hydrogel Matrix to Support Stem Cell Survival After Brain Transplantation in Stroke. Neurorehab and Neural Repair 24(7): 636-644.

Zhu, Z., L. Zheng, Y. Li, T. Huang, Y. C. Chao, L. Pan, H. Zhu, Y. Zhao, W. Yu & P. Li (2019) Potential Immunotherapeutic Targets on Myeloid Cells for Neurovascular Repair After Ischemic Stroke. Front Neurosci, 13, 758.

Zierath, D., A. Kunze, L. Fecteau & K. Becker (2015) Promiscuity of autoimmune responses to MBP after stroke. J Neuroimmunol, 285, 101-5.

Zou, X., X. J. Yang, Y. M. Gan, D. L. Liu, C. Chen, W. Duan & J. R. Du (2021) Neuroprotective Effect of Phthalide Derivative CD21 against Ischemic Brain Injury:Involvement of MSR1 Mediated DAMP peroxiredoxin1 Clearance and TLR4 Signaling Inhibition. J Neuroimmune Pharmacol, 16, 306-317.